Investigation of the Interaction Between Cdc42 and its Effector TOCA1: Handover of Cdc42 to the Actin Regulator N-WASP is Facilitated by Differential Binding Affinities.

Joanna R. Watson[1], Helen M. Fox[1,2], Daniel Nietlispach[1], Jennifer L. Gallop[1,2], Darerca Owen[1]* & Helen R. Mott[1]*

From [1] the Department of Biochemistry, 80, Tennis Court Road, Cambridge CB2 1GA. UK and [2] the Wellcome Trust/Cancer Research UK Gurdon Institute University of Cambridge, Cambridge, CB2 1QN, UK.

Running title: *Investigation of the TOCA1-Cdc42 interaction*

*To whom correspondence should be addressed: Dr H. R. Mott, Department of Biochemistry, 80, Tennis Court Road, Cambridge CB2 1GA, UK, Telephone 44-1223-764825, Fax 44-1223-766002, Email hrm28@cam.ac.uuk or Dr D. Owen, Department of Biochemistry, 80, Tennis Court Road, Cambridge CB2 1GA, UK, Telephone 44-1223-764824, Fax 44-1223-766002, Email do202@cam.ac.uk

Keywords: CDC42; endocytosis; actin; NMR; protein-protein interaction

ABSTRACT

Transducer of Cdc42-dependent actin assembly protein 1 (TOCA1) is an effector of the Rho family small G protein Cdc42. It contains a membrane-deforming F-BAR domain as well as an SH3 domain and a G protein-binding HR1 (homology region 1) domain. TOCA1 binding to Cdc42 leads to actin rearrangements, which are thought to be involved in processes such as endocytosis, filopodia formation and cell migration. We have solved the structure of the HR1 domain of TOCA1, providing the first structural data for this protein. We have found that the TOCA1 HR1, like the closely related CIP4 HR1, has interesting structural features that are not observed in other HR1 domains. We have also investigated the binding of the TOCA HR1 domain to Cdc42, and the potential ternary complex between Cdc42 and the G protein binding regions of TOCA1 and a member of the Wiskott-Aldrich syndrome protein family, N-WASP. TOCA1 binds Cdc42 with micromolar affinity, in contrast to the nanomolar affinity of the N-WASP G protein binding region for Cdc42. NMR experiments show that the Cdc42 binding domain from N-WASP is able to displace TOCA1 HR1 from Cdc42, while the N-WASP domain but not the TOCA1 HR1 domain inhibits actin polymerisation. This suggests that TOCA1 binding to Cdc42 is an early step in the Cdc42-dependent pathways that govern actin dynamics and the differential binding affinities of the effectors facilitate a handover from TOCA1 to N-WASP, which can then drive recruitment of the actin modifying machinery.

INTRODUCTION

The Ras superfamily of small GTPases comprises over 150 members that regulate a multitude of cellular processes in eukaryotes. The superfamily can be divided into five families based on structural and

functional similarities: Ras, Rho, Rab, Arf and Ran. All members share a well-defined core structure of ~20 kDa known as the G domain, which is responsible for guanine nucleotide binding (1). It is this guanine nucleotide binding that underlies their function as molecular switches, controlling a vast array of signalling pathways. These molecular switches cycle between active, GTP-bound, and inactive, GDP-bound, states with the help of auxiliary proteins. The guanine nucleotide exchange factors mediate formation of the active state by promoting the dissociation of GDP, allowing GTP to bind. The GTPase activating proteins stimulate the rate of intrinsic GTP-hydrolysis, mediating the return to the inactive state (reviewed in 2).

The overall conformation of small G proteins in the active and inactive states is similar but they differ significantly in two main regions known as switch I and switch II. These regions are responsible for 'sensing' the nucleotide-state, with the GTP-bound state showing greater rigidity and the GDP-bound state adopting a more relaxed conformation (reviewed in 3). In the active state, G proteins bind to an array of downstream effectors, through which they exert their extensive roles within the cell. The structures of more than 60 small G protein-effector complexes have been solved and, not surprisingly, the switch regions have been implicated in a large proportion of the G protein-effector interactions (reviewed in 4). However, as each of the 150 members of the superfamily interacts with multiple effectors, there are still a huge number of known G protein-effector interactions that have not yet been studied structurally.

The Rho family comprises 20 members, of which three, RhoA, Rac1 and Cdc42, have been relatively well studied. The role of these three proteins in the coordination of the actin cytoskeleton has been extensively examined (5–10). RhoA acts to rearrange existing actin structures to form stress fibres, while Rac1 and Cdc42 promote *de novo* actin polymerisation to form lamellipodia and filopodia respectively (9–12). A number of RhoA and Rac1 effector proteins, including the Formins (13) and members of the Protein Kinase C-related Kinase (PRK)[1] family (14), along with Cdc42 effectors including the Wiskott-Aldrich Syndrome (WASP) family (15) and the transducer of Cdc42-dependent actin assembly (TOCA) family (16–18) have also been linked to the pathways that govern cytoskeletal dynamics.

Cdc42 effectors, TOCA1 and the ubiquitously expressed member of the WASP family, N-WASP, have been implicated in the regulation of actin polymerisation downstream of Cdc42 and phosphatidylinositol 4,5-bisphosphate [$PI(4,5)P_2$] (9, 16, 19–22). N-WASP exists in an autoinhibited conformation, which is released upon $PI(4,5)P_2$ and Cdc42 binding (21, 23) or by other factors such as phosphorylation (24). Following their release, the C-terminal regions of N-WASP are free to interact with G-actin and a known nucleator of actin assembly, the Arp2/3 complex (25). The importance of TOCA1 in actin polymerisation has been demonstrated in a range of *in vitro* and *in vivo* studies (16, 26–32) but the exact role of TOCA1 in the many pathways involving actin assembly remains unclear. The most widely studied role of TOCA1 is in membrane invagination and endocytosis (28–30, 33, 34), although it has also been implicated in filopodia formation (27), neurite elongation (35), transcriptional reprogramming via nuclear actin (36) and interaction with ZO-1 at tight junctions (37). A role in cell motility and invasion has also been established (38, 39).

TOCA1 comprises an N-terminal F-BAR domain, a central homology region 1 (HR1) domain and a C-terminal SH3 domain. The F-BAR domain is a known dimerisation, membrane-binding and membrane-deforming module (33, 40, 41) found in a number of cell signalling proteins. The TOCA1 SH3 domain has many known binding partners, including N-WASP (16) and Dynamin (40). The HR1 domain has been directly implicated in the interaction between TOCA1 and Cdc42 (16), representing the first Cdc42-HR1 domain interaction to be identified.

Other HR1 domains studied so far, including those from the PRK family, have

been found to bind their cognate Rho family G protein-binding partner with high specificity and affinities in the nanomolar range (42–45). The structures of the PRK1 HR1a domain in complex with RhoA (42) and the HR1b domain in complex with Rac1 (46) show that the HR1 domain comprises an anti-parallel coiled-coil that interacts with its G protein binding partner via both helices. Both of the G protein switch regions are involved in the interaction. The coiled-coil fold is shared by the HR1 domain of the TOCA family protein, CIP4 (47) and, based on sequence homology, by TOCA1 itself. These HR1 domains, however, show specificity for Cdc42, rather than RhoA or Rac1 (16, 17). How different HR1 domain proteins distinguish their specific G protein partners remains only partially understood and structural characterisation of a novel G protein-HR1 domain interaction would add to the growing body of information pertaining to these protein complexes. Furthermore, the biological function of the interaction between TOCA1 and Cdc42 remains poorly understood and so far there has been no biophysical or structural insight.

The interactions of TOCA1 and N-WASP with Cdc42 as well as with each other has raised questions as to whether the two Cdc42-effectors can interact with a single molecule of Cdc42 simultaneously. There is some evidence for a ternary complex between Cdc42, N-WASP and TOCA1 (30) but there was no direct demonstration of simultaneous contacts between the two effectors and a single molecule of Cdc42. Nonetheless, the substantially different structures of the G protein binding regions of the two effectors is intriguing, and implies that they bind to Cdc42 quite differently, providing motivation for investigating the possibility that Cdc42 can bind both effectors concurrently. WASP interacts with Cdc42 via a conserved, unstructured binding motif known as the Cdc42- and Rac-interactive binding region (CRIB) (48), which forms an intermolecular β-sheet, expanding the anti-parallel β2 ad β3 strands of Cdc42 (49). In contrast, the TOCA family proteins are thought to interact via the HR1 domain, which may form a triple coiled-coil with switch II of Rac1, like the HR1b domain of PRK1 (46).

Here, we present the solution NMR structure of the HR1 domain of TOCA1, providing the first structural data for this protein. We also present data pertaining to binding of the TOCA HR1 domain to Cdc42, which is the first biophysical description of an HR1 domain binding this particular Rho-family small G protein. Finally, we investigate the potential ternary complex between Cdc42 and the G protein-binding regions of TOCA1 and N-WASP, contributing to our understanding of G protein-effector interactions as well as the roles of Cdc42, N-WASP and TOCA1 in the pathways that govern actin dynamics.

EXPERIMENTAL PROCEDURES

Expression Constructs - *Xenopus tropicalis* TOCA1 HR1 domain (residues 330-426 and N-terminally extended constructs as indicated) were amplified from cDNA (TOCA1 accession number NM_001005148) and cloned into pGEX-6P-1 (GE Healthcare) or pGEX-HisP (44). The HR1 domain of human CIP4 (residues 388-481) was amplified from IMAGE:3532036, the *Xenopus laevis* FBP17 HR1 domain (residues 385-486) from IMAGE: 5514481 and the *Xenopus tropicalis* N-WASP/WASL GBD (residues 197-255) from IMAGE: 5379332 and all were cloned into pGEX-6P-1. The resulting constructs express the proteins as N-terminal GST-fusions with a 3C protease-cleavable tag, with pGEX-HisP expressing an additional C-terminal His_6-tag. Human Cdc42Δ7Q61L and full-length Cdc42 were cloned into pGEX-2T (GE Healthcare) and pGEX-6P-1 respectively. A C-terminally extended construct of TOCA1 comprising residues 330-545 was cloned into pMAT10-P (D. Owen, unpublished). The resulting construct expresses TOCA1 330-545 as an N-terminal His-MBP fusion protein with a 3C protease-cleavable tag. Full-length *Xenopus tropicalis* TOCA1, TOCA1 F-BAR (residues 1-287) and TOCA1 ΔSH3 (residues 1-480) were PCR amplified from a cDNA clone (IMAGE: 5157175) and cloned into pET-6xHis-SNAP using *Fse*I and *Asc*I sites

that had been incorporated into the primers to create His-SNAP-TOCA1 proteins.

Protein Expression – GST fusion proteins (HR1 domains and Cdc42) were expressed in *E. coli* BL21 cells (Invitrogen). Stationary cultures were diluted 1 in 10 and grown at 37 °C until an A_{600} ~ 0.8 was reached, then induced with 0.1 mM isopropyl-β-D-thiogalactopyranoside for 20 hours at 20 °C. The GST-N-WASP GBD construct was expressed in *E. coli* BL21-CodonPlus®-RIL (Agilent Technologies). The proteins were purified using glutathione-agarose beads (Sigma) and eluted from the beads by cleavage of the GST-tag with 3C protease (HR1 domains, N-WASP GBD and full-length Cdc42Q61L) or Thrombin (Novagen, Cdc42Δ7Q61L) prior to gel filtration on a 16/60 S75 column (GE Healthcare). His-MBP-HR1-SH3 was purified using nickel-NTA-agarose beads (Life Technologies) prior to cleavage with 3C protease and gel filtration. Full-length TOCA1, TOCA1 F-BAR and TOCA1 ΔSH3 were expressed from pET-6xHis-SNAP in BL21 pLysS, grown at 37 °C until an A_{600} of ~ 0.6 was reached and induced with 0.3 mM isopropyl-β-D-thiogalactopyranoside overnight at 19 °C. Proteins were coupled to Ni-NTA-agarose (Qiagen), eluted using increasing concentrations of imidazole and further purified by gel filtration using a 16/60 S200 column (GE Healthcare). All protein concentrations were determined by amino acid analysis (PNAC Facility, Department of Biochemistry, University of Cambridge).

Nucleotide Exchange - For NMR experiments, Cdc42 was nucleotide exchanged for the non-hydrolysable GTP analogue GMPPNP (Sigma) as described previously (50). For SPAs, Cdc42 was loaded with [^{3}H]GTP using [8-^{3}H]GTP (Perkin Elmer) as described previously (51). The protein was confirmed as full-length using mass spectrometry (PNAC facility, Department of Biochemistry, University of Cambridge).

Scintillation Proximity Assays (SPAs) - Direct: GST-PAK, GST-ACK or His-tagged TOCA1 constructs were attached to a fluromicrosphere via an anti-GST or anti-His antibody in the presence of Cdc42Δ7Q61L·[^{3}H]GTP. Binding curves were fitted using a direct binding isotherm to obtain K_d values and their curve-fitting errors for the G protein-effector interactions (52). Competition: free ACK GBD, TOCA1 HR1, TOCA1 HR1SH3 or N-WASP GBD were titrated into a mixture of 30 nM Cdc42Δ7Q61L·[^{3}H]GTP and 30 nM GST-ACK immobilised on a fluromicrosphere as above. Data were fitted to competition binding isotherms to obtain K_d values and curve-fitting errors, as described previously (53).

NMR Spectroscopy - The NMR experiments and resonance assignments of the HR1 domain are described (54). The NMR experiments were carried out with 0.9 mM ^{13}C/^{15}N-labelled HR1 domain in 20 mM sodium phosphate pH 7.5, 150 mM NaCl, 5 mM $MgCl_2$, 5 mM DTT, 10 % D_2O. Distance restraints were derived from a ^{15}N-separated NOESY (100 msec mixing time) recorded on a Bruker DRX500 and a ^{13}C-separated NOESY (100 msec mixing time) recorded on an Avance AV600. NMR data were processed using *AZARA* (W. Boucher), University of Cambridge and analysed using *ANALYSIS* (55).

Structure Calculation - Structures were calculated iteratively using CNS 1.0 interfaced to Aria2.3.1 (56). The PROSLQ force field was used for non-bonded parameters. Backbone torsion angles were estimated from CA, CO, CB, N and HA chemical shifts using TALOS-N (57) .The "strong" ϕ and ψ restraints were included with an error of ± 2 standard deviations of the averaged TALOS-N predictions. Dihedral angle predictions for residues 323-340 were weak and so no restraints were included for this region.

NMR Titrations - All of the ^{15}N- and ^{13}C-HSQCs were recorded at 25 ˚C in 50 mM sodium phosphate pH 5.5, 25 mM NaCl, 5 mM $MgCl_2$, 5 mM DTT, 10 % D_2O on a Bruker DRX500. ^{15}N-HR1 HSQC experiments were recorded on 0.2 mM ^{15}N-HR1 domain with HR1:Cdc42·GMPPNP ratios of 1:0, 1:0.25, 1:0.5, 1:1 and 1:4. Experiments were recorded on 0.27 mM ^{15}N-Cdc42·GMPPNP at

Cdc42:HR1 ratios of 1:0, 1:0.25, 1:0.5 and 1:2.2. The ^{15}N-HSQC titrations with N-WASP were recorded on 0.6 mM ^{15}N-HR1 domain or 0.15 mM ^{15}N-Cdc42 at the ratios indicated in the figures.

Chemical Shift Mapping - The chemical shift changes, δ, were calculated using the equation:

$$\delta = \sqrt{\delta_{^1H}^2 + (0.15\delta_{^{15}N})^2}$$

where d^1_H and d^{15}_N are the chemical shift changes for the ^{1}H and ^{15}N dimensions respectively. Residues that had disappeared were assigned a δ value larger than the maximum calculated δ for the data set and residues that were too overlapped to be reliably assigned in the complex spectra were assigned δ = 0. The residues that had shifted more than the mean chemical shift change across the spectrum were classed as significant and were filtered for solvent accessibility using *NACCESS* (58). Residues with less than 50 % solvent accessibility were considered to be buried and unavailable for binding.

Pyrene actin assays - Pyrene actin assays were carried out as previously described in (59). *Xenopus* high speed supernatant was used at 5 mg/mL and supplemented with 0.12 mg/mL pyrene actin as described previously (32). TOCA1 HR1 domain or N-WASP CRIB domain was added at the concentrations indicated. Liposomes were made using previously described methods (60), from 60 % phosphatidylcholine, 30 % phosphatidylserine and 10 % PI(4,5)P_2 to 2 mM final lipid concentration. All of the lipids used were natural brain or liver lipids from Avanti Polar Lipids. The assays were initiated by addition of 5 μL of liposomes per 200 μL of reaction mix.

RESULTS

Cdc42-TOCA1 Binding

TOCA1 was identified in *Xenopus* extracts as a protein necessary for Cdc42-dependent actin assembly (16) and was shown to bind to Cdc42·GTPγS but not to Cdc42·GDP or to Rac1 and RhoA. Given its homology to other Rho-family binding modules, it is likely that the HR1 domain of TOCA1 is sufficient to bind Cdc42. The *C. elegans* TOCA1 orthologues also bind to Cdc42 via their consensus HR1 domain (34). The HR1 domains from the PRK family bind their G protein partners with a high affinity, exhibiting a range of sub-micromolar dissociation constants (K_d) as low as 26 nM (45). A K_d in the nM range was therefore expected for the interaction of the TOCA1 HR1 domain with Cdc42.

We generated a *X. tropicalis* TOCA1 HR1 domain construct encompassing residues 330-426. This region comprises the complete HR1 domain based on secondary structure predictions and sequence alignments with another TOCA family member, CIP4, whose structure has been determined (47). The interaction between [^{3}H]GTP·Cdc42 and a C-terminally His-tagged TOCA1 HR1 domain construct was investigated using scintillation proximity assays (SPA). The binding isotherm for the interaction is shown in Figure 1A, together with the Cdc42-PAK interaction as a positive control (52). The binding of TOCA1 HR1 to Cdc42 was unexpectedly weak, with a K_d > 1 μM. It was not possible to estimate the K_d more accurately using direct SPA experiments, as saturation could not be reached due to non-specific signal at higher protein concentrations.

It was possible that the low affinity observed was due to negative effects of immobilization of the HR1 domain and so other methods were employed, which utilized untagged proteins. Isothermal titration calorimetry was carried out but no heat changes were observed at a range of concentrations and temperatures (data not shown), suggesting that the interaction is predominantly entropically driven. Other G protein-HR1 domain interactions have also failed to show heat changes in our hands (DO, unpublished data). Infrared interferometry with immobilized Cdc42 was also attempted, but was unsuccessful for both TOCA1 HR1 and for the positive control, ACK.

The affinity was therefore determined using competition SPAs. A complex of a GST-fusion of the G protein binding domain (GBD) of ACK, which binds with a high

affinity to Cdc42 (61), with radiolabelled [^{3}H]GTP·Cdc42 was pre-formed and the effect of increasing concentrations of untagged TOCA1 HR1 domain was examined. Competition of GST-ACK bound to [^{3}H]GTP·Cdc42 by free ACK GBD was used as a control and to establish the value of background counts when Cdc42 is fully displaced. The data were fitted to a binding isotherm describing competition (53). Free ACK competed with itself with an affinity of 32 nM, similar to the value obtained by direct binding of 23 nM (61). The TOCA1 HR1 domain also fully competed with the GST-ACK but bound with an affinity of 6 μM (Figure 1B and C), in agreement with the low affinity observed in the direct binding experiments.

The Cdc42 construct used in the binding assays has 7 residues deleted from the C-terminus to facilitate purification. These residues are not generally required for G protein-effector interactions, including the interaction between RhoA and the PRK1 HR1a domain (53). In contrast, the C-terminus of Rac1 contains a polybasic sequence, which is crucial for Rac1 binding to the HR1b domain from PRK1 (43, 46). As the observed affinity between TOCA1 HR1 and Cdc42 was much lower than expected, we reasoned that the C-terminus of Cdc42 might be necessary for a high affinity interaction. The binding experiments were repeated with full-length [^{3}H]GTP·Cdc42 but the affinity of the HR1 domain for full-length Cdc42 was similar to its affinity for truncated Cdc42 ($K_d \approx 5$ μM, Figure 1C). Thus, the C-terminal region of Cdc42 is not required for maximal binding of TOCA1 HR1.

Another possible explanation for the low affinities observed was that the HR1 domain alone is not sufficient for maximal binding of the TOCA proteins to Cdc42 and that the other domains are required. Indeed, GST-pull downs performed with *in vitro* translated human TOCA1 fragments had suggested that residues N-terminal to the HR1 domain may be required to stabilize the HR1 domain structure (16). Furthermore, both BAR and SH3 domains have been implicated in interactions with small G proteins *e.g.* the BAR domain of Arfaptin2 binds to Rac1 and Arl1 (62) while an SH3 domain mediates the interaction between Rac1 and the guanine nucleotide exchange factor, β-PIX (63). TOCA1 dimerizes via its F-BAR domain, which could also affect Cdc42 binding, for example by presenting two HR1 domains for Cdc42 interactions. Various TOCA1 fragments (Figure 2A) were therefore assessed for binding to full-length Cdc42 by direct SPA. The isolated F-BAR domain showed no binding to full-length Cdc42 (Figure 2B). Full-length TOCA1 and ΔSH3 TOCA1 bound with micromolar affinity (Figure 2B), in a similar manner to the isolated HR1 domain (Figure 1A). The HR1-SH3 protein could not be purified to homogeneity as a fusion protein so was assayed in competition assays after cleavage of the His tag. This construct competed with GST-ACK GBD to give a similar affinity to the HR1 domain alone (K_d = 4.6 ± 4 μM, Figure 2C). Taken together, these data suggest that the TOCA1 HR1 domain is sufficient for maximal binding and that this binding is of a relatively low affinity compared to many other Cdc42-effector complexes.

The low affinity of the TOCA1 HR1-Cdc42 interaction raised the question as to whether the other known Cdc42-binding TOCA family proteins, FBP17 (18) and CIP4 (17), also bind weakly. The HR1 domains from FBP17 and CIP4 were purified and assayed for Cdc42 binding in competition SPAs, analogous to those carried out with the TOCA1 HR1 domain. The affinity of both the FBP17 and CIP4 HR1 domains were also in the low micromolar range (10 and 5 μM respectively) (Figure 2D and E), suggesting that low affinity interactions with Cdc42 are a common feature within the TOCA family.

Structure of the TOCA1 HR1 Domain

As the TOCA1 HR1 domain was sufficient for maximal Cdc42-binding, we used this construct for structural studies. Initial experiments were performed with TOCA1 residues 324-426 but we observed that the N-terminus was cleaved during purification to

yield a new N-terminus at residue 330 (data not shown). We therefore engineered a construct comprising residues 330-426 to produce the minimal, stable HR1 domain. Backbone and sidechain resonances were assigned as described (54). 2,778 non-degenerate NOE restraints were used in initial structure calculations (1,791 unambiguous and 987 ambiguous), derived from 3D ^{15}N-separated NOESY and ^{13}C-separated NOESY experiments. There were 1,845 unambiguous NOEs and 757 ambiguous NOEs after 8 iterations. 100 structures were calculated in the final iteration, the 50 lowest energy structures were water refined and of these the 35 lowest energy structures were analysed. Table 1 indicates that the HR1 domain structure is well defined by the NMR data.

The structure closest to the mean is shown in Figure 3A. The two α-helices of the HR1 domain interact to form an anti-parallel coiled-coil with a slight left-handed twist, reminiscent of the HR1 domains of CIP4 (47) (PDB Code:2KE4) and PRK1 (42, 43) (PDB Codes:1CXZ,1URF). A sequence alignment illustrating the secondary structure elements of the TOCA1 and CIP4 HR1 domains and the HR1a and HR1b domains from PRK1 is shown in Figure 3B.

In the HR1a domain of PRK1, a region N-terminal to helix 1 forms a short α-helix, which packs against both helices of the HR1 domain (42). This region of TOCA1 HR1 (residues 334-340) is well defined in the family of structures (Figure 3A) but does not form an α-helix. It instead forms a series of turns, defined by NOE restraints observed between residues separated by one (332-334, 333-335 etc.) or two (337-340) residues in the sequence and the ϕ and ψ angles, assessed using Stride (64). These turns cause the chain to reverse direction, allowing the N-terminal segment (334-340) to contact both helices of the HR1 domain. Long range NOEs were observed linking Leu334, Glu335 and Asp336 with Trp413 of helix 2, Leu334 with Lys409 of helix 2, and Phe337 and Ser338 with Arg345, Arg348 and Leu349 of helix 1. These contacts are summarized in Figure 3C.

The two α-helices of TOCA1 HR1 are separated by a long loop of ten residues (380-389) that contains two short 3_{10} helices (residues 381-383 and 386-389). Interestingly, sidechains of residues within the loop region point back towards helix 1; for example, there are numerous distinct NOEs between the sidechains of Asn380 and Met383 of the loop region and Tyr377 and Val376 of helix 1 (Figure 3D). The backbone NH and CHα groups of Gly384 and Asp385 also show NOEs with the sidechain of Tyr377.

Mapping the TOCA1 and Cdc42 Binding Interfaces

The HR1^{TOCA1}-Cdc42 interface was investigated using NMR spectroscopy. A series of ^{15}N-HSQC experiments was recorded on ^{15}N-labelled TOCA1 HR1 domain in the presence of increasing concentrations of unlabelled Cdc42Δ7Q61L·GMPPNP to map the Cdc42-binding surface. A comparison of the ^{15}N-HSQC spectra of free HR1 and HR1 in the presence of excess Cdc42 shows that although some peaks were shifted, several were much broader in the complex and a considerable subset had disappeared (Figure 4A). This behaviour cannot be explained by the increase in molecular mass (from 12 kDa to 33 kDa) when Cdc42 binds and is more likely to be due to conformational exchange. This leads to broadening of the peaks so that they are not detectable. Overall chemical shift perturbations (CSP) were calculated for each residue, while those that had disappeared were assigned a shift change of 0.2 (Figure 4B). A peak that disappeared or had a CSP above the mean CSP for the spectrum was considered to be significantly affected.

^{15}N-HSQC shift mapping experiments report on changes to amide groups, which are mainly inaccessible as they are buried inside the helices and are involved in hydrogen bonds. Therefore, ^{13}C-HSQC and methyl-selective SOFAST-HMQC (65) experiments were also recorded on ^{15}N,^{13}C-labelled TOCA1 HR1 to yield more information on sidechain involvement. The affected CH groups underwent significant line broadening, similarly to the NH peaks. Sidechains whose

CH groups disappeared in the presence of Cdc42 are marked on the graph in Figure 4B with green asterisks.

TOCA1 residues whose signals were affected by Cdc42 binding were mapped onto the structure of TOCA1 HR1 (Figure 4C). The changes were localized to one end of the coiled-coil and the binding site appeared to include residues from both α-helices and the loop region that joins them. Residues outside this region were not significantly affected, indicating that there was no widespread conformational change. The residues in the interhelical loop and helix 1 that contact each other (Figure 3D) show shift changes in their backbone NH and sidechains in the presence of Cdc42. For example, the sidechain of Asn380, and the backbones of Val376 and Tyr377 were significantly affected but are all buried in the free TOCA1 HR1 structure, indicating that local conformational changes in the loop may facilitate complex formation. The chemical shift mapping data indicate that the G protein binding region of the TOCA1 HR1 domain is broadly similar to that of the CIP4 and PRK1 HR1 domains (Figure 4D; Figure 3B).

The corresponding ^{15}N- and ^{13}C-NMR experiments were also recorded on ^{15}N-Cdc42Δ7Q61L·GMPPNP or ^{15}N/^{13}C - Cdc42Δ7Q61L·GMPPNP in the presence of unlabelled HR1 domain. The overall CSP was calculated for each residue. As was the case when labelled HR1 was observed, several peaks were shifted in the complex but many disappeared, indicating exchange on an unfavourable, millisecond timescale (Figure 5A). Detailed sidechain data could not be obtained for all residues due to spectral overlap but constant-time ^{13}C-HSQC and methyl-selective SOFAST-HMQC experiments provided further information on certain, well-resolved sidechains (marked with green asterisks in Figure 5B).

As many of the peaks disappeared, the mean chemical shift change was relatively low and so a threshold of the mean plus one standard deviation was used to define a significant CSP. Residues that disappeared were also classed as significantly affected. Parts of the switch regions (Figure 5B, C) are invisible in NMR spectra recorded on free Cdc42 due to conformational exchange. These switch regions become visible in Cdc42 and other small G protein-effector complexes (46, 61, 66) due to a decrease in conformational freedom upon complex formation. The switch regions of Cdc42 did not, however, become visible in the presence of the TOCA1 HR1 domain. Indeed, Ser30 of switch I and Arg66, Arg68, Leu70 and Ser71 of switch II are visible in free Cdc42 but disappear in the presence of the HR1 domain. This suggests that the switch regions are not rigidified in the HR1 complex and are still in conformational exchange. Nevertheless, mapping of the affected residues onto the NMR structure of free Cdc42Δ7Q61L·GMPPNP (Figure 5C, HRM and DO, unpublished) shows that although they are relatively widespread compared to changes in the HR1 domain in general they are on the face of the protein that includes the switches. Although the binding interface may be overestimated, this suggests that the switch regions are involved in binding to TOCA1.

Modelling the Cdc42-TOCA1 HR1 Complex

The Cdc42-HR1^{TOCA1} complex was not amenable to full structural analysis due to the weak interaction and the extensive exchange broadening seen in the NMR experiments. HADDOCK (67) was, therefore, used to perform rigid body docking based on the structures of free HR1 domain and Cdc42 and ambiguous interaction restraints derived from the titration experiments described above. Residues with significantly affected resonances and more than 50 % solvent accessibility were defined as active. Passive residues were defined automatically as those neighbouring active residues.

The orientation of the HR1 domain with respect to Cdc42 cannot be definitively concluded in the absence of unambiguous distance restraints and hence HADDOCK produced a set of models in which the HR1 domain contacts the same surface on Cdc42 but is in various orientations with respect to Cdc42. The cluster with the lowest RMSD

from the lowest energy structure is assumed to be the best model. By these criteria, in the best model the HR1 domain is in a similar orientation to the HR1a domain of PRK1 bound to RhoA and the HR1b domain bound to Rac1. A representative model from this cluster is shown in Figure 6A alongside the Rac1-HR1b structure (46) (PDB Code:2RMK) in Figure 6B.

A sequence alignment of RhoA, Cdc42 and Rac1 is shown in Figure 6C. The RhoA and Rac1 contact residues in the switch regions are invisible in the spectra of Cdc42 but they are generally conserved between all three G proteins. Several Cdc42 residues identified by chemical shift mapping are not in close contact in the Cdc42-TOCA1 model (Figure 6A). Some of these can be rationalized, for example, $Thr24^{Cdc42}$, $Leu160^{Cdc42}$ and $Lys163^{Cdc42}$ all pack behind switch I and are likely to be affected by conformational changes within the switch, while $Glu95^{Cdc42}$, $Lys96^{Cdc42}$ are in the helix behind switch II. Other residues that are affected in the Cdc42-TOCA1 complex but that do not correspond to contact residues of RhoA or Rac1 (Figure 6C) include $Gln2^{Cdc42}$, $Lys16^{Cdc42}$, $Thr52^{Cdc42}$ and $Arg68^{Cdc42}$. $Lys16^{Cdc42}$ is unlikely to be a contact residue as it is involved in nucleotide binding but the others may represent specific Cdc42-TOCA1 contacts. In the model these sidechains are involved in direct contacts (Figure 6D).

Competition between N-WASP and TOCA1

From the known interactions and effects of the proteins in biological systems, it has been suggested that TOCA1 and N-WASP could bind Cdc42 simultaneously (16). Studies in CHO cells indicated that a Cdc42-N-WASP-TOCA1 complex existed (30), since FRET was observed between RFP-TOCA1 and GFP-N-WASP and the efficiency was decreased when an N-WASP mutant was used that no longer binds Cdc42. An overlay of the HADDOCK model of the Cdc42-$HR1^{TOCA1}$ complex and the structure of Cdc42 in complex with the GBD of the N-WASP homologue, WASP (49) (PDB Code: 1CEE), shows that the HR1 and GBD binding sites only partly overlap and, therefore, a ternary complex remained possible (Figure 7A). Interestingly, the presence of the TOCA1 HR1 would not prevent the core CRIB of WASP from binding to Cdc42, although the regions C-terminal to the CRIB that are required for high affinity binding of WASP (68) would interfere sterically with the TOCA1 HR1. A basic region in WASP including three lysines (230-232), N-terminal to the core CRIB, has been implicated in an electrostatic steering mechanism (69) and these residues would be free to bind in the presence of TOCA1 HR1 (Figure 7A).

An N-WASP GBD construct was produced and its affinity for Cdc42 measured by competition SPA (Figure 7B). The K_d that was determined (37 nM) is consistent with the previously reported affinity (69). Unlabelled N-WASP GBD was titrated into ^{15}N-Cdc42Δ7Q61L·GMPPNP and the backbone NH groups monitored using HSQCs (Figure 7C). Unlabelled $HR1^{TOCA1}$ was then added to the Cdc42-N-WASP complex and no changes were seen, suggesting that the N-WASP GBD was not displaced even in the presence of a 5-fold excess of $HR1^{TOCA1}$. These experiments were recorded at suffciently high protein concentrations (145 μM Cdc42, 145 μM N-WASP GBD, 725 μM TOCA1 HR1 domain) to be far in excess of the K_ds of the individual interactions (TOCA1 $K_d \approx 5$ μM, N-WASP K_d = 37 nM). A comparison of the HSQC experiments recorded on ^{15}N-Cdc42 alone, in the presence of TOCA1 HR1, N-WASP GBD, or both, shows that the spectra in the presence of N-WASP and in the presence of both N-WASP and TOCA1 HR1 are identical (Figure 7C).

Furthermore, ^{15}N-TOCA1 HR1 was monitored in the presence of unlabelled Cdc42Δ7Q61L·GMPPNP (1:1) before and after addition of 0.25 and 1.0 equivalents of unlabelled N-WASP GBD. The spectrum when N-WASP and TOCA1 were equimolar was identical to that of the free HR1 domain, while the spectrum in the presence of 0.25 equivalents of N-WASP was intermediate between the TOCA1 HR1 free and complex spectra (Figure 7D). When in fast exchange,

the NMR signal represents a population-weighted average between free and bound states and so the intermediate spectrum indicates that the population comprises a mixture of free and bound HR1 domain. Hence a third, intermediate state that includes all three proteins is unlikely. Again, the experiments were recorded on protein samples far in excess of the individual K_ds (600 μM of each protein). These data indicate that the HR1 domain is displaced from Cdc42 by N-WASP and that a ternary complex comprising TOCA1 HR1, N-WASP GBD and Cdc42 is not formed. Taken together, the data in Figure 7C and D indicate unidirectional competition for Cdc42 binding in which the N-WASP GBD displaces TOCA1 HR1 but not *vice versa*.

To extend these studies to a more complex system and to assess the ability of TOCA1 HR1 to compete with full length N-WASP, pyrene actin assays were employed. These assays, described in detail elsewhere, (59) were carried out using pyrene actin-supplemented *Xenopus* extracts into which exogenous TOCA1 HR1 domain or N-WASP GBD was added, to assess their effects on actin polymerisation. Actin polymerisation in all cases was initiated by the addition of PI(4,5)P_2-containing liposomes. Actin polymerisation triggered by addition of PI(4,5)P_2-containing liposomes has previously been shown to depend on TOCA1 and N-WASP (32). Endogenous N-WASP is present at approximately 100 nM in *Xenopus* extracts, while TOCA1 is present at 10-fold lower concentration than N-WASP (16).

Addition of the isolated N-WASP GBD significantly inhibited the polymerisation of actin at concentrations as low as 100 nM and completely abolished polymerisation at higher concentrations (Figure 8). The GBD presumably acts as a dominant negative, sequestering endogenous Cdc42 and preventing endogenous full-length N-WASP from binding and becoming activated. The addition of the TOCA1 HR1 domain to 100 μM had no significant effect on the rate of actin polymerisation or maximum fluorescence. This is consistent with endogenous N-WASP, activated by other components of the assay, outcompeting the TOCA1 HR1 domain for Cdc42-binding.

DISCUSSION

The Cdc42-TOCA1 interaction

The TOCA1 HR1 domain alone is sufficient for Cdc42-binding *in vitro* and yet the affinity of the TOCA1 HR1 domain for Cdc42 is remarkably low ($K_d \approx 5$ μM). This is over 100x lower than that of the N-WASP GBD (K_d = 37 nM) and considerably lower than other known G protein-HR1 domain interactions. The polybasic tract within the C-terminal region of Cdc42 does not appear to be required for binding to TOCA1, which is in contrast to the interaction between Rac1 and the HR1b domain of PRK1 but more similar to the PRK1 HR1a-RhoA interaction. A single binding interface on both the HR1 domain and Cdc42 can be concluded from the data presented here. Furthermore, the interfaces are comparable to those of other G protein-HR1 interactions (Figure 4) and the lowest energy model produced in rigid body docking resembles previously studied G protein-HR1 complexes (Figure 6). It seems, therefore, that the interaction, despite its relatively low affinity, is specific and sterically similar to other HR1 domain-G protein interactions.

The TOCA1 HR1 domain is a left-handed coiled-coil comparable to other known HR1 domains (42, 43, 47). A short region N-terminal to the coiled-coil exhibits a series of turns and contacts residues of both helices of the coiled-coil (Figure 3). The corresponding sequence in CIP4 also includes a series of turns but is flexible, while in the HR1a domain of PRK1 the equivalent region adopts an α-helical structure that packs against the coiled-coil. The contacts between the N-terminal region and the coiled-coil are predominantly hydrophobic in both cases, but sequence specific contacts do not appear to be conserved. This region is distant from the G protein-binding interface of the HR1 domains, so the structural differences may relate to the structure and regulation of these domains, rather than their G protein interactions.

The inter-helical loops of TOCA1 and CIP4 differ from the same region in the HR1 domains of PRK1 in that they are longer and contain two short stretches of 3_{10}-helix. This region lies within the G protein-binding surface of all of the HR1 domains (Figure 4D). TOCA1 and CIP4 both bind weakly to Cdc42, whereas the HR1a domain of PRK1 binds tightly to RhoA and Rac1 and the HR1b domain to Rac1. The structural features shared by TOCA1 and CIP4 may therefore be related to Cdc42-binding specificity and the low affinities. In free TOCA1, the sidechains of the inter-helical region make extensive contacts with residues in helix 1. Many of these residues are significantly affected in the presence of Cdc42 and so it is likely that the conformation of this loop is altered in the Cdc42 complex. These observations therefore provide a molecular mechanism whereby mutation of $Met^{383}Gly^{384}Asp^{385}$ to $Ile^{383}Ser^{384}Thr^{385}$ abolishes TOCA1 binding to Cdc42 (16).

The lowest energy model produced by HADDOCK using ambiguous interaction restraints from the titration data resembled the NMR structures of RhoA and Rac1 in complex with their HR1 domain partners (42, 46). Some speculative conclusions can be made based on this model. For example, $Phe56^{Cdc42}$, which is not visible in free Cdc42 or Cdc42-$HR1^{TOCA1}$, is close to the TOCA1 HR1 (Figure 6A). $Phe56^{Cdc42}$, which is a Trp in both Rac1 and RhoA (Figure 6C), is thought to pack behind switch I when Cdc42 interacts with ACK, maintaining the switch in a binding-competent orientation (70). This residue has also been identified as important for Cdc42-WASP binding (71). $Phe56^{Cdc42}$ is therefore likely to be involved in the Cdc42-TOCA1 interaction, probably by stabilising the position of switch I.

Some residues that are affected in the Cdc42-$HR1^{TOCA1}$ complex, but do not correspond to contact residues of RhoA or Rac1 (Figure 6C), may contact $HR1^{TOCA1}$ directly (Figure 6D). $Gln2^{Cdc42}$, which has also been identified as a contact residue in the Cdc42-ACK complex (61), contacts $Val376^{TOCA1}$ and $Asn380^{TOCA1}$ in the model and disrupts the contacts between the interhelical loop and the first helix of the TOCA1 coiled-coil. $Thr52^{Cdc42}$, which has also been identified as making minor contacts with ACK (61, 72), falls near the sidechains of $HR1^{TOCA1}$ helix 1, particularly $Lys372^{TOCA1}$, while the equivalent position in Rac1 is $Asn52^{Rac1}$. N52T is one of a combination of seven residues found to confer ACK-binding on Rac1 (72) and so may represent a specific Cdc42-effector contact residue. The position equivalent to $Lys372^{TOCA1}$ in PRK1 is $Glu58^{HR1a}$ or $Gln151^{HR1b}$. $Thr52^{Cdc42}$-$Lys372^{TOCA1}$ may therefore represent a specific Cdc42-$HR1^{TOCA1}$ contact. $Arg68^{Cdc42}$ of switch II is positioned close to $Glu395^{TOCA1}$ (Figure 6D), suggesting a direct electrostatic contact between switch II of Cdc42 and helix 2 of the HR1 domain. The equivalent Arg in Rac1 and RhoA is pointing away from the HR1 domains of PRK1. The importance of this residue in the Cdc42-TOCA1 interaction remains unclear, although its mutation reduces binding to RhoGAP, suggesting that it can be involved in Cdc42 interactions (53).

The solution structure of the TOCA1 HR1 domain presented here, along with the model of the $HR1^{TOCA1}$-Cdc42 complex is consistent with a conserved mode of binding across the known HR1 domain-Rho family interactions, despite their differing affinities. The weak binding prevented detailed structural and thermodynamic studies of the complex. Nonetheless, structural studies of the TOCA1 HR1 domain, combined with chemical shift mapping, have highlighted some potentially interesting differences between Cdc42-$HR1^{TOCA1}$ and RhoA/Rac1-$HR1^{PRK1}$ binding.

We have previously postulated that the inherent flexibility of HR1 domains contributes to their ability to bind to different Rho family G proteins, with Rho binding HR1 domains displaying increased flexibility, reflected in their lower melting temperatures (T_m) and Rac binders being more rigid (44, 45). The T_m of the TOCA1 HR1 domain is 61.9 °C (data not shown), which is the highest T_m that we have measured for an HR1 domain thus far. As such the ability of the TOCA1

HR1 domain to bind to Cdc42 (a close relative of Rac1 rather than RhoA) fits this trend. An investigation into the local motions, particularly in the G protein binding regions, may offer further insight into the differential specificities and affinities of G protein-HR1 domain interactions.

Significance of a weak, transient interaction

The low affinity of the Cdc42-HR1^{TOCA1} interaction is consistent with a tightly spatially and temporally regulated pathway, requiring combinatorial signals leading to a series of coincident weak interactions that elicit full activation. The HR1 domains from other TOCA family members, CIP4 and FBP17, also bind at low micromolar affinities to Cdc42 and so the low affinity interaction appears to be commonplace among this family of HR1 domain proteins, in contrast to the PRK family. Weak, transient protein-protein interactions are functionally significant in several systems (73–75), for example, the binding of adaptor proteins to protein cargo during the formation of clathrin-coated vesicles in endocytosis involves multiple interactions of micromolar affinity (76, 77).

The low affinity of the HR1^{TOCA1}-Cdc42 interaction in the context of the physiological concentration of TOCA1 in *Xenopus* extracts (approximately 10 nM) (16) suggests that binding between TOCA1 and Cdc42 is likely to occur *in vivo* only when TOCA1 is at high local concentrations and membrane localized, and therefore in close proximity to activated Cdc42. Evidence suggests that the TOCA family of proteins are recruited to the membrane via an interaction between their F-BAR domain and specific signalling lipids. For example, electrostatic interactions between the F-BAR domain and the membrane are required for TOCA1 recruitment to membrane vesicles and tubules (27) and TOCA1-dependent actin polymerisation is known to depend specifically on PI(4,5)P_2 (32). Furthermore, the isolated F-BAR domain of FBP17 has been shown to induce membrane tubulation of brain liposomes and BAR domain proteins that promote tubulation cluster on membranes at high densities (33). Once at the membrane, high local concentrations of TOCA1 could exceed the K_d of F-BAR dimerisation (likely to be comparable to that of the FCHo2 F-BAR domain (2.5 μM) (41)) and that of the Cdc42-HR1^{TOCA1} interaction. Cdc42-HR1^{TOCA1} binding would then be favourable, as long as coincident activation of Cdc42 had occurred, leading to stabilization of TOCA1 at the membrane and downstream activation of N-WASP.

It has been postulated that WASP and N-WASP exist in equilibrium between folded (inactive) and unfolded (active) forms and the affinity of Cdc42 for the unfolded WASP proteins is significantly enhanced (78). The unfolded, high affinity state of WASP is represented by a short peptide, the GBD, which binds with a low nM affinity to Cdc42 (49). In contrast, the best estimate of the affinity of full-length WASP for Cdc42 is low micromolar (79), In the inactive state of WASP, the actin- and Arp2/3-binding VCA domain contacts the GBD (21, 23, 80), competing for Cdc42 binding. The high affinity of Cdc42 for the unfolded, active form pushes the equilibrium in favour of (N-)WASP activation. Binding of PI(4,5)P_2 to the basic region just N-terminal to the GBD further favours the active conformation (21). A substantial body of data has illuminated the complex regulation of WASP/N-WASP proteins and current evidence suggests that these allosteric activation mechanisms and oligomerization combine to regulate WASP activity, allowing the synchronization and integration of multiple potential activation signals (reviewed in 24). Our data are easily reconciled with this model.

We envisage that TOCA1 is first recruited to the appropriate membrane in response to PI(4,5)P_2 via its F-BAR domain, where the local increase in concentration favours F-BAR mediated dimerization of TOCA1. Cdc42 is activated in response to co-incident signals and can then bind to TOCA1, further stabilising TOCA1 at the membrane. TOCA1 can then recruit N-WASP (26) via an interaction between its SH3 domain and the N-

WASP proline-rich region (16). The recruitment of N-WASP alone and of the N-WASP/WIP complex by TOCA1 and FBP17 has been demonstrated (26). WIP inhibits the activation of N-WASP by Cdc42, an effect that is reversed by TOCA1 (16). It may, therefore, be envisaged that WIP and TOCA1 exert opposing allosteric effects on N-WASP, with TOCA1 favouring the unfolded, active conformation of N-WASP and increasing its affinity for Cdc42. TOCA1 may also activate N-WASP by effective oligomerization, as clustering of TOCA1 at the membrane following coincident interactions with $PI(4,5)P_2$ and Cdc42 would in turn lead to clustering of N-WASP, in addition to pushing the equilibrium towards the unfolded, active state.

In a cellular context full-length TOCA1 and N-WASP are likely to have similar affinities for active Cdc42 but in the unfolded, active conformation, the affinity of N-WASP for Cdc42 dramatically increases. Our binding data suggests that TOCA1 HR1 binding is not allosterically regulated and our NMR data, along with the high stability of TOCA1 HR1, suggest that there is no widespread conformational change in the presence of Cdc42. As full-length TOCA1 and the isolated HR1 domain bind Cdc42 with similar affinities, the N-WASP-Cdc42 interaction will be favoured as the N-WASP GBD can easily outcompete the TOCA1 HR1 for Cdc42. A combination of allosteric activation by $PI(4,5)P_2$, activated Cdc42 and TOCA1 and oligomeric activation implemented by TOCA1 would lead to full activation of N-WASP and downstream actin polymerisation.

In such an array of molecules localised to a discrete region of the membrane, it is plausible that WASP could bind to a second Cdc42 molecule, rather than displacing TOCA1 from its cognate Cdc42. Our NMR and affinity data, however, are consistent with displacement of the TOCA1 HR1 by the N-WASP GBD. Furthermore, TOCA1 is required for Cdc42-mediated activation of N-WASP/WIP (16), implying that it may not be possible for Cdc42 to bind and activate N-WASP prior to TOCA1-Cdc42 binding. The commonly used MGD→IST (Cdc42-binding deficient) mutant of TOCA1 has a reduced ability to activate the N-WASP/WIP complex (26), further indicating the importance of the Cdc42-$HR1^{TOCA1}$ interaction prior to downstream activation of N-WASP.

In light of this, we favour an 'effector handover' scheme whereby TOCA1 interacts with Cdc42 prior to N-WASP activation, after which N-WASP displaces TOCA1 from its bound Cdc42 in order to be fully activated, rather than binding a second Cdc42 molecule. Potentially the TOCA1-Cdc42 interaction functions to position N-WASP and Cdc42 such that they are poised to interact with high affinity. The concomitant release of TOCA1 from Cdc42 while still bound to N-WASP presumably enhances the ability of TOCA1 to further activate N-WASP/WIP-induced actin polymerisation. There is an advantage to such an 'effector handover', since N-WASP would only be robustly recruited when F-BAR domains are already present. Hence, actin polymerisation cannot occur until F-BAR domains are poised for membrane distortion.

Our model of the Cdc42-$HR1^{TOCA1}$ complex indicates a mechanism by which such a handover could take place (Figure 9), as it shows that the effector binding sites only partially overlap on Cdc42. The lysine residues thought to be involved in an electrostatic steering mechanism in WASP-Cdc42 binding (69) are conserved in N-WASP and would be able to interact with Cdc42 even when the TOCA1 HR1 domain is already bound. It has been postulated that the initial interactions between this basic region and Cdc42 could stabilise the active conformation of WASP, leading to high affinity binding between the core CRIB and Cdc42 (68). The region C-terminal to the core CRIB, required for maximal affinity binding (68), would then fully displace the TOCA1 HR1.

In conclusion, the data presented here show that the TOCA1 HR1 domain is sufficient for Cdc42-binding *in vitro* and that the interaction is of micromolar affinity, lower than that of other G protein-HR1 domain interactions. The analogous HR1 domains

from other TOCA1 family members FBP17 and CIP4 also exhibit micromolar affinity for Cdc42. A role for the TOCA1-, FBP17- and CIP4-Cdc42 interactions in the recruitment of these proteins to the membrane therefore appears unlikely. Instead, our findings agree with earlier suggestions that the F-BAR domain is responsible for membrane-recruitment (27, 33). The role of the Cdc42-TOCA1 interaction remains somewhat elusive but may serve to position activated Cdc42 and N-WASP to allow full activation of N-WASP, and as such serve to couple F-BAR mediated membrane deformation with N-WASP activation. We envisage a complex interplay of equilibria between free and bound, active and inactive Cdc42, TOCA family and WASP family proteins, facilitating a tightly spatially and temporally regulated pathway requiring numerous simultaneous events in order to achieve appropriate and robust activation of the downstream pathway. Our data is, therefore, easily reconciled with the dynamic instability models described in relation to the formation of endocytotic vesicles (75) and with the current data pertaining to the complex activation of WASP/N-WASP pathways by allosteric and oligomeric effects (24).

It is clear from the data presented here that TOCA1 and N-WASP do not bind Cdc42 simultaneously and that N-WASP is likely to outcompete TOCA1 for Cdc42-binding. We, therefore, postulate an effector handover mechanism based on current evidence surrounding WASP/N-WASP activation and our model of the Cdc42-HR1^{TOCA1} complex. The displacement of the TOCA1 HR1 domain from Cdc42 by N-WASP may represent a unidirectional step in the pathway of Cdc42/N-WASP/TOCA1-dependent actin assembly.

Acknowledgements
JRW is supported by a Herchel Smith studentship. JLG is supported by a Wellcome Trust Research Career Development Fellowship (WT095829AIA), European Research Council Starting Grant (281971) and Gurdon Institute funding provided by the Wellcome Trust (092096) and CRUK (C6946/A14492). HMF is supported by a Wellcome Trust PhD Studentship (WT099740Z12Z). We would like to thank Dr A Walrant for help with the pyrene actin assays and liposome preparation. We are also grateful to Dr J.R. Peterson (Fox Chase Cancer Center) for human TOCA1 clones.

Conflict of Interest
The authors declare that they have no conflicts of interest with the contents of this article.

Author Contributions
JRW generated constructs and proteins, set up NMR experiments, analysed NMR data and performed binding experiments, HMF generated longer TOCA clones and proteins, DN set up NMR experiments, JLG supervised the pyrene actin assays, DO supervised the protein binding assays, HRM performed NMR experiments and analysed NMR data. JRW, DO and HRM wrote the paper with input from all authors.

REFERENCES

1. Bourne, H. R., Sanders, D. A., and McCormick, F. (1991) The GTPase superfamily: conserved structure and molecular mechanism. *Nature*. **349**, 117–127
2. Cherfils, J., and Zeghouf, M. (2013) Regulation of small GTPases by GEFs, GAPs, and GDIs. *Physiol. Rev.* **93**, 269–309
3. Vetter, I. R., and Wittinghofer, A. (2001) The guanine nucleotide-binding switch in three dimensions. *Science.* **294**, 1299–1304
4. Mott, H. R., and Owen, D. (2015) Structures of Ras superfamily effector complexes: What have we learnt in two decades? *Crit. Rev. Biochem. Mol. Biol.* **50**, 85–133
5. Machesky, L. M., and Hall, A. (1996) Rho: a connection between membrane receptor signalling and the cytoskeleton. *Trends Cell Biol.* **6**, 304–310
6. Ridley, A. J., and Hall, A. (1992) The small GTP-binding protein rho regulates the assembly of focal adhesions and actin stress fibers in response to growth factors. *Cell*. **70**, 389–399
7. Ridley, A. J., Paterson, H. F., Johnston, C. L., Diekmann, D., and Hall, A. (1992) The small GTP-binding protein rac regulates growth factor-induced membrane ruffling. *Cell*. **70**, 401–410
8. Ridley, A. J. (1996) Rho: theme and variations. *Curr. Biol.* **6**, 1256–1264
9. Nobes, C. D., and Hall, A. (1995) Rho, Rac, and Cdc42 GTPases regulate the assembly of multimolecular focal complexes associated with actin stress fibers, lamellipodia, and filopodia. *Cell*. **81**, 53–62
10. Hall, A. (1998) Rho GTPases and the Actin Cytoskeleton. *Science.* **279**, 509–514
11. Machesky, L. M., and Insall, R. H. (1999) Signaling to Actin Dynamics. *J. Cell Biol.* **146**, 267–272
12. Kozma, R., Ahmed, S., Best, A., and Lim, L. (1995) The Ras-related protein Cdc42Hs and bradykinin promote formation of peripheral actin microspikes and filopodia in Swiss 3T3 fibroblasts. *Mol. Cell. Biol.* **15**, 1942–1952
13. Kühn, S., and Geyer, M. (2014) Formins as effector proteins of Rho GTPases. *Small GTPases*. **5**, e983876
14. Watanabe, G., Saito, Y., Madaule, P., Ishizaki, T., Fujisawa, K., Morii, N., Mukai, H., Ono, Y., Kakizuka, A., and Narumiya, S. (1996) Protein Kinase N (PKN) and PKN-Related Protein Rhophilin as Targets of Small GTPase Rho. *Science.* **271**, 645–648
15. Symons, M., Derry, J. M. ., Karlak, B., Jiang, S., Lemahieu, V., McCormick, F., Francke, U., and Abo, A. (1996) Wiskott-Aldrich syndrome protein, a novel effector for the GTPase CDC42Hs, is implicated in actin polymerization. *Cell*. **84**, 723–734
16. Ho, H. H., Rohatgi, R., Lebensohn, A. M., Le Ma, Li, J., Gygi, S. P., and Kirschner, M. W. (2004) Toca-1 mediates Cdc42-dependent actin nucleation by activating the N-WASP-WIP complex. *Cell*. **118**, 203–216
17. Aspenström, P. (1997) A Cdc42 target protein with homology to the non-kinase domain of FER has a potential role in regulating the actin cytoskeleton. *Curr. Biol.* **7**, 479–487
18. Wu, M., Wu, X., and De Camilli, P. (2013) Calcium oscillations-coupled

conversion of actin travelling waves to standing oscillations. *Proc. Natl. Acad. Sci. U.S.A.* **110**, 1339–1344
19. Miki, H., Suetsugu, S., and Takenawa, T. (1998) WAVE, a novel WASP-family protein involved in actin reorganization induced by Rac. *EMBO J.* **17**, 6932–6941
20. Rohatgi, R., Ma, L., Miki, H., Lopez, M., Kirchhausen, T., Takenawa, T., and Kirschner, M. W. (1999) The Interaction between N-WASP and the Arp2/3 Complex Links Cdc42-Dependent Signals to Actin Assembly. *Cell*. **97**, 221–231
21. Rohatgi, R., Ho, H. Y., and Kirschner, M. W. (2000) Mechanism of N-WASP activation by CDC42 and phosphatidylinositol 4, 5-bisphosphate. *J. Cell Biol.* **150**, 1299–1310
22. Cantley, L. C., Janmey, P. A., and Kirschner, M. W. (1998) Corequirement of Specific Phosphoinositides and Small GTP-binding Protein Cdc42 in Inducing Actin Assembly in Xenopus Egg Extracts. *J. Cell Biol.* **140**, 1125–1136
23. Kim, A. S., Kakalis, L. T., Abdul-Manan, N., Liu, G. A., and Rosen, M. K. (2000) Autoinhibition and activation mechanisms of the Wiskott–Aldrich syndrome protein. *Nature*. **404**, 151–158
24. Padrick, S. B., and Rosen, M. K. (2010) Physical mechanisms of signal integration by WASP family proteins. *Annu. Rev. Biochem.* **79**, 707–735
25. Ma, L., Rohatgi, R., and Kirschner, M. W. (1998) The Arp2/3 complex mediates actin polymerization induced by the small GTP-binding protein Cdc42. *Proc. Natl. Acad. Sci. U.S.A.* **95**, 15362–15367
26. Takano, K., Takano, K., Toyooka, K., and Suetsugu, S. (2008) EFC/F-BAR proteins and the N-WASP-WIP complex induce membrane curvature-dependent actin polymerization. *EMBO J.* **27**, 2817–2828
27. Bu, W., Chou, A. M., Lim, K. B., Sudhaharan, T., and Ahmed, S. (2009) The Toca-1-N-WASP complex links filopodial formation to endocytosis. *J. Biol. Chem.* **284**, 11622–11636
28. Fricke, R., Gohl, C., Dharmalingam, E., Grevelhörster, A., Zahedi, B., Harden, N., Kessels, M., Qualmann, B., and Bogdan, S. (2009) Drosophila Cip4/Toca-1 Integrates Membrane Trafficking and Actin Dynamics through WASP and SCAR/WAVE. *Curr. Biol.* **19**, 1429–1437
29. Giuliani, C., Troglio, F., Bai, Z., Patel, F. B., Zucconi, A., Malabarba, M. G., Disanza, A., Stradal, T. B., Cassata, G., Confalonieri, S., Hardin, J. D., Soto, M. C., Grant, B. D., and Scita, G. (2009) Requirements for F-BAR Proteins TOCA-1 and TOCA-2 in Actin Dynamics and Membrane Trafficking during Caenorhabditis elegans Oocyte Growth and Embryonic Epidermal Morphogenesis. *PLoS Genet.* **5**, e1000675
30. Bu, W., Lim, K. B., Yu, Y. H., Chou, A. M., Sudhaharan, T., and Ahmed, S. (2010) Cdc42 interaction with N-WASP and Toca-1 regulates membrane tubulation, vesicle formation and vesicle motility: implications for endocytosis. *PLoS One*. **5**, 1–16
31. Lee, K., Gallop, J. L., Rambani, K., and Kirschner, M. W. (2010) Self-Assembly of Filopodia-Like Structures on Supported Lipid Bilayers. *Science.* **329**, 1341–1345
32. Gallop, J. L., Walrant, A., Cantley, L. C., and Kirschner, M. W. (2013) Phosphoinositides and membrane curvature switch the mode of actin

polymerization via selective recruitment of toca-1 and Snx9. *Proc. Natl. Acad. Sci. U.S.A.* **110**, 7193–7198

33. Tsujita, K., Suetsugu, S., Sasaki, N., Furutani, M., Oikawa, T., and Takenawa, T. (2006) Coordination between the actin cytoskeleton and membrane deformation by a novel membrane tubulation domain of PCH proteins is involved in endocytosis. *J. Cell Biol.* **172**, 269–279
34. Bai, Z., and Grant, B. D. (2015) A TOCA/CDC-42/PAR/WAVE functional module required for retrograde endocytic recycling. *Proc. Natl. Acad. Sci. U.S.A.* **112**, E1443–1452
35. Kakimoto, T., Katoh, H., and Negishi, M. (2006) Regulation of Neuronal Morphology by Toca-1, an F-BAR/EFC Protein That Induces Plasma Membrane Invagination. *J. Biol. Chem.* **281**, 29042–29053
36. Miyamoto, K., Pasque, V., Jullien, J., and Gurdon, J. B. (2011) Nuclear actin polymerization is required for transcriptional reprogramming of Oct4 by oocytes. *Genes Dev.* **25**, 946–958
37. Van Itallie, C. M., Tietgens, A. J., Krystofiak, E., Kachar, B., and Anderson, J. M. (2015) A complex of ZO-1 and the BAR-domain protein TOCA-1 regulates actin assembly at the tight junction. *Mol. Biol. Cell*. **26**, 2769–2787
38. Hu, J., Mukhopadhyay, A., and Craig, A. W. B. (2011) Transducer of Cdc42-dependent actin assembly promotes epidermal growth factor-induced cell motility and invasiveness. *J. Biol. Chem.* **286**, 2261–2272
39. Chander, H., Truesdell, P., Meens, J., and Craig, a W. B. (2013) Transducer of Cdc42-dependent actin assembly promotes breast cancer invasion and metastasis. *Oncogene*. **32**, 3080–3090
40. Itoh, T., Erdmann, K. S., Roux, A., Habermann, B., Werner, H., and De Camilli, P. (2005) Dynamin and the actin cytoskeleton cooperatively regulate plasma membrane invagination by BAR and F-BAR proteins. *Dev. Cell*. **9**, 791–804
41. Henne, W. M., Kent, H. M., Ford, M. G. J., Hegde, B. G., Daumke, O., Butler, P. J. G., Mittal, R., Langen, R., Evans, P. R., and McMahon, H. T. (2007) Structure and analysis of FCHo2 F-BAR domain: a dimerizing and membrane recruitment module that effects membrane curvature. *Structure*. **15**, 839–852
42. Maesaki, R., Ihara, K., Shimizu, T., Kuroda, S., Kaibuchi, K., and Hakoshima, T. (1999) The Structural Basis of Rho Effector Recognition Revealed by the Crystal Structure of Human RhoA Complexed with the Effector Domain of PKN/PRK1. *Mol. Cell*. **4**, 793–803
43. Owen, D., Lowe, P. N., Nietlispach, D., Brosnan, C. E., Chirgadze, D. Y., Parker, P. J., Blundell, T. L., and Mott, H. R. (2003) Molecular dissection of the interaction between the small G proteins Rac1 and RhoA and protein kinase C-related kinase 1 (PRK1). *J. Biol. Chem.* **278**, 50578–50587
44. Hutchinson, C. L., Lowe, P. N., McLaughlin, S. H., Mott, H. R., and Owen, D. (2011) Mutational Analysis Reveals a Single Binding Interface between RhoA and Its Effector, PRK1. *Biochemistry*. **50**, 2860–2869
45. Hutchinson, C. L., Lowe, P. N., McLaughlin, S. H., Mott, H. R., and Owen, D. (2013) Differential binding of RhoA, RhoB, and RhoC to protein kinase C-related kinase (PRK) isoforms PRK1, PRK2, and PRK3: PRKs have the highest affinity for RhoB. *Biochemistry*. **52**, 7999–8011

46. Modha, R., Campbell, L. J., Nietlispach, D., Buhecha, H. R., Owen, D., and Mott, H. R. (2008) The Rac1 polybasic region is required for interaction with its effector PRK1. *J. Biol. Chem.* **283**, 1492–1500
47. Kobashigawa, Y., Kumeta, H., Kanoh, D., and Inagaki, F. (2009) The NMR structure of the TC10- and Cdc42-interacting domain of CIP4. *J. Biomol. NMR*. **44**, 113–118
48. Burbelo, P., Drechsel, D., and Hall, A. (1995) A Conserved Binding Motif Defines Numerous Candidate Target Proteins for Both Cdc42 and Rac GTPases. *J. Biol. Chem.* **270**, 29071–29074
49. Abdul-Manan, N., Aghazadeh, B., Liu, G. A., Majumdar, A., Ouerfelli, O., Siminovitch, K. A., and Rosen, M. K. (1999) Structure of Cdc42 in complex with the GTPase-binding domain of the "Wiskott-Aldrich syndrome" protein. *Nature*. **399**, 379–383
50. Owen, D., Mott, H. R., Laue, E. D., and Lowe, P. N. (2000) Residues in Cdc42 That Specify Binding to Individual CRIB Effector Proteins. *Biochemistry*. **39**, 1243–1250
51. Bailey, L. K., Campbell, L. J., Evetts, K. a, Littlefield, K., Rajendra, E., Nietlispach, D., Owen, D., and Mott, H. R. (2009) The structure of binder of Arl2 (BART) reveals a novel G protein binding domain: implications for function. *J. Biol. Chem.* **284**, 992–999
52. Thompson, G., Owen, D., Chalk, P. A., and Lowe, P. N. (1998) Delineation of the Cdc42/Rac-binding domain of p21-activated kinase. *Biochemistry*. **37**, 7885–7891
53. Owen, D., Campbell, L. J., Littlefield, K., Evetts, K. A., Li, Z., Sacks, D. B., Lowe, P. N., and Mott, H. R. (2008) The IQGAP1-Rac1 and IQGAP1-Cdc42 interactions: interfaces differ between the complexes. *J. Biol. Chem.* **283**, 1692–1704
54. Watson, J. R., Nietlispach, D., Owen, D., and Mott, H. R. (2016) (1)H, (13)C and (15)N resonance assignments of the Cdc42-binding domain of TOCA1. *Biomol. NMR Assign.* 10.1007/s12104-016-9677-8
55. Vranken, W. F., Boucher, W., Stevens, T. J., Fogh, R. H., Pajon, A., Llinas, M., Ulrich, E. L., Markley, J. L., Ionides, J., and Laue, E. D. (2005) The CCPN data model for NMR spectroscopy: development of a software pipeline. *Proteins*. **59**, 687–696
56. Rieping, W., Habeck, M., Bardiaux, B., Bernard, A., Malliavin, T. E., and Nilges, M. (2007) ARIA2: automated NOE assignment and data integration in NMR structure calculation. *Bioinformatics*. **23**, 381–382
57. Shen, Y., and Bax, A. (2013) Protein backbone and sidechain torsion angles predicted from NMR chemical shifts using artificial neural networks. *J. Biomol. NMR*. **56**, 227–241
58. Hubbard, S., and Thornton, J. (1993) NACCESS, Computer Program. Department of Biochemistry Molecular Biology, University College London.
59. Walrant, A., Saxton, D. S., Correia, G. P., and Gallop, J. L. (2015) Triggering actin polymerization in Xenopus egg extracts from phosphoinositide-containing lipid bilayers. *Methods Cell Biol.* **128**, 125–147
60. Lebensohn, A. M., and Kirschner, M. W. (2009) Activation of the WAVE Complex by Coincident Signals Controls Actin Assembly. *Mol. Cell*. **36**, 512–524

61. Mott, H. R., Owen, D., Nietlispach, D., Lowe, P. N., Manser, E., Lim, L., and Laue, E. D. (1999) Structure of the small G protein Cdc42 bound to the GTPase-binding domain of ACK. *Nature*. **399**, 384–388
62. Nakamura, K., Man, Z., Xie, Y., Hanai, A., Makyio, H., Kawasaki, M., Kato, R., Shin, H.-W., Nakayama, K., and Wakatsuki, S. (2012) Structural basis for membrane binding specificity of the Bin/Amphiphysin/Rvs (BAR) domain of Arfaptin-2 determined by Arl1 GTPase. *J. Biol. Chem.* **287**, 25478–25489
63. ten Klooster, J. P., Jaffer, Z. M., Chernoff, J., and Hordijk, P. L. (2006) Targeting and activation of Rac1 are mediated by the exchange factor beta-Pix. *J. Cell Biol.* **172**, 759–769
64. Heinig, M., and Frishman, D. (2004) STRIDE: a web server for secondary structure assignment from known atomic coordinates of proteins. *Nucleic Acids Res.* **32**, W500–502
65. Schanda, P., Kupce, E., and Brutscher, B. (2005) SOFAST-HMQC experiments for recording two-dimensional heteronuclear correlation spectra of proteins within a few seconds. *J. Biomol. NMR*. **33**, 199–211
66. Fenwick, R. B., Campbell, L. J., Rajasekar, K., Prasannan, S., Nietlispach, D., Camonis, J., Owen, D., and Mott, H. R. (2010) The RalB-RLIP76 Complex Reveals a Novel Mode of Ral-Effector Interaction. *Structure*. **18**, 985–995
67. de Vries, S. J., van Dijk, M., and Bonvin, A. M. J. J. (2010) The HADDOCK web server for data-driven biomolecular docking. *Nat. Protoc.* **5**, 883–897
68. Rudolph, M. G., Bayer, P., Abo, A., Kuhlmann, J., Vetter, I. R., and Wittinghofer, A. (1998) The Cdc42/Rac interactive binding region motif of the Wiskott Aldrich syndrome protein (WASP) is necessary but not sufficient for tight binding to Cdc42 and structure formation. *J. Biol. Chem.* **273**, 18067–18076
69. Hemsath, L., Dvorsky, R., Fiegen, D., Carlier, M.-F., and Ahmadian, M. R. (2005) An electrostatic steering mechanism of Cdc42 recognition by Wiskott-Aldrich syndrome proteins. *Mol. Cell*. **20**, 313–324
70. Elliot-Smith, A. E., Owen, D., Mott, H. R., and Lowe, P. N. (2007) Double Mutant Cycle Thermodynamic Analysis of the Hydrophobic Cdc42−ACK Protein−Protein Interaction. *Biochemistry*. **46**, 14087–14099
71. Wang, J., Lu, Q., and Lu, H. P. (2006) Single-molecule dynamics reveals cooperative binding-folding in protein recognition. *PLoS Comput. Biol.* **2**, 842–852
72. Elliot-Smith, A. E., Mott, H. R., Lowe, P. N., Laue, E. D., and Owen, D. (2005) Specificity determinants on Cdc42 for binding its effector protein ACK. *Biochemistry*. **44**, 12373–12383
73. Perkins, J. R., Diboun, I., Dessailly, B. H., Lees, J. G., and Orengo, C. (2010) Transient protein-protein interactions: structural, functional, and network properties. *Structure*. **18**, 1233–1243
74. Acuner Ozbabacan, S. E., Engin, H. B., Gursoy, A., and Keskin, O. (2011) Transient protein-protein interactions. *Protein Eng. Des. Sel.* **24**, 635–648
75. Schmid, E. M., and McMahon, H. T. (2007) Integrating molecular and network biology to decode endocytosis. *Nature*. **448**, 883–888
76. Praefcke, G. J. K., Ford, M. G. J., Schmid, E. M., Olesen, L. E., Gallop, J. L., Peak-Chew, S.-Y., Vallis, Y., Babu, M. M., Mills, I. G., and McMahon, H. T.

(2004) Evolving nature of the AP2 alpha-appendage hub during clathrin-coated vesicle endocytosis. *EMBO J.* **23**, 4371–4383

77. Höning, S., Ricotta, D., Krauss, M., Späte, K., Spolaore, B., Motley, A., Robinson, M., Robinson, C., Haucke, V., and Owen, D. J. (2005) Phosphatidylinositol-(4,5)-bisphosphate regulates sorting signal recognition by the clathrin-associated adaptor complex AP2. *Mol. Cell*. **18**, 519–531
78. Leung, D. W., and Rosen, M. K. (2005) The nucleotide switch in Cdc42 modulates coupling between the GTPase-binding and allosteric equilibria of Wiskott-Aldrich syndrome protein. *Proc. Natl. Acad. Sci. U.S.A*. **102**, 5685–5690
79. Buck, M., Xu, W., and Rosen, M. K. (2004) A two-state allosteric model for autoinhibition rationalizes WASP signal integration and targeting. *J. Mol. Biol.* **338**, 271–285
80. Miki, H., and Takenawa, T. (1998) Direct binding of the verprolin-homology domain in N-WASP to actin is essential for cytoskeletal reorganization. *Biochem. Biophys. Res. Commun.* **243**, 73–78

FOOTNOTES

[1] The abbreviations used are:
PRK – protein kinase C related kinase; WASP – Wiskott-Aldrich syndrome protein; TOCA – transducer of Cdc42-dependent actin assembly protein; N-WASP – Neural Wiskott-Aldrich syndrome protein; $PI(4,5)P_2$ - phosphatidylinositol 4,5-bisphosphate; HR1 – homology region 1; F-BAR – Fes/CIP4 homology BAR; SH3 – Src-homology 3; CRIB – Cdc42- and Rac- interactive binding; CIP4 – Cdc42-interacting protein 4; GST – Glutathione S-transferase; MBP – maltose binding protein; GBD – G protein binding domain; SPA – scintillation proximity assay; PAK – p21-activated kinase; ACK – activated Cdc42-associated kinase; NOESY – nuclear Overhauser effect spectroscopy; HSQC – heteronuclear single quantum correlation; NOE – nuclear Overhauser effect.

The atomic coordinates (code 5FRG) have been deposited in the Protein Data Bank, Research Collaboratory for Structural Bioinformatics, Rutgers University, New Brunswick, NJ (http://www.rcsb.org/).

FIGURE LEGENDS

FIGURE 1. The TOCA1 HR1-Cdc42 interaction is low affinity. A, The curves derived from direct binding assays in which the indicated concentrations of Cdc42Δ7Q61L·[^{3}H]GTP were incubated with 30 nM GST-PAK or HR1-His_6 in SPAs. The SPA signal was corrected by subtraction of control data with no GST-PAK or HR1-His_6. The data were fitted to a binding isotherm to give an apparent K_d and are expressed as a percentage of the maximum signal; B, C, Competition SPA experiments were carried out with the indicated concentrations of (B) ACK GBD or (C) HR1 domain titrated into 30 nM GST-ACK and either 30 nM Cdc42Δ7Q61L·[^{3}H]GTP or full-length Cdc42Q61L·[^{3}H]GTP. The K_d values derived for the ACK GBD with Cdc42Δ7 and FL were 0.032 ± 0.01 and 0.011 ± 0.01 μM respectively. The K_d values derived for the TOCA1 HR1 with Cdc42Δ7 and FL were 6.05 ± 1.96 and 5.39 ± 1.69 μM respectively.

FIGURE 2. The Cdc42-HR1 interaction is of low affinity in the context of full length protein and in TOCA1 paralogues. A, A diagram illustrating the TOCA1 constructs assayed for Cdc42 binding. Domain boundaries are derived from secondary structure predictions; B, The binding

curves derived from direct binding assays, in which the indicated concentrations of Cdc42Δ7Q61L·[^{3}H]GTP were incubated with 30 nM GST-ACK or His-tagged TOCA1 constructs as indicated, in SPAs. The SPA signal was corrected by subtraction of control data with no fusion protein. The data were fitted to a binding isotherm to give an apparent K_d and are expressed as a percentage of the maximum signal; C,D,E, Representative examples of competition SPA experiments carried out with indicated concentrations of (C) the TOCA1 HR1-SH3 construct titrated into 30 nM GST-ACK and 30 nM Cdc42Δ7Q61L·[^{3}H]GTP, (D) HR1^{CIP4} or (E) HR1^{FBP17} titrated into 30 nM GST-ACK and 30 nM Cdc42FLQ61L·[^{3}H]GTP.

FIGURE 3. The structure of the TOCA1 HR1 domain. A, The backbone trace of the 35 lowest energy structures of the HR1 domain overlaid with the structure closest to the mean is shown alongside a cartoon representation of the structure closest to the mean. Flexible regions at the N- and C-termini (330-333 and 421-426) are omitted for clarity; B, A sequence alignment of the HR1 domains from TOCA1, CIP4 and PRK1. The secondary structure was deduced using Stride (64), based on the Ramachandran angles, and is indicated as follows; grey = turn, yellow = α-helix, blue = 3_{10} helix, white = coil; C, A close-up of the N-terminal region of TOCA1 HR1, indicating some of the NOEs defining its position with respect to the two α-helices. Dotted lines indicate NOE restraints; D, A close-up of the interhelix loop region showing some of the contacts between the loop and helix 1. NOEs are indicated with dotted lines. All structural figures were generated using PYMOL (http://pymol.sourceforge.net).

FIGURE 4. Mapping the binding surface of Cdc42 onto the TOCA1 HR1 domain. A, The ^{15}N-HSQC of 200 μM TOCA1 HR1 domain is shown in the free form (black) and in the presence of a 4-fold molar excess of Cdc42Δ7Q61L·GMPPNP (red). Expansions of two regions are shown with peak assignments, showing backbone amides in fast or intermediate exchange; B, Chemical shift perturbations (CSP) were calculated as described in Materials and Methods and are shown for backbone and sidechain NH groups. The mean CSP is marked with a red line. Residues that disappeared in the presence of Cdc42 were assigned a CSP of 0.2 but excluded when calculating the mean CSP and are indicated with open bars. Those that were not traceable due to spectral overlap were assigned a CSP of zero and are marked with an asterisk below the bar. Residues with affected sidechain CSPs derived from ^{13}C HSQCs are marked with green asterisks above the bars. Secondary structure elements are shown below the graph; C, A cartoon representation of the HR1 domain. Residues with significantly affected backbone or sidechain chemical shifts when Cdc42 bound and that are buried are coloured dark blue, while those that are solvent accessible are coloured yellow. Residues with significantly affected backbone and sidechain groups that are solvent accessible are coloured red. A close up of the binding region is shown, with affected sidechain heavy atoms shown as sticks; D, The G protein-binding region is marked in red onto structures of the HR1 domains as indicated.

FIGURE 5. Mapping the binding surface of the HR1 domain onto Cdc42. A, The ^{15}N-HSQC of Cdc42Δ7Q61L·GMPPNP is shown in its free form (black) and in the presence of excess TOCA1 HR1 domain (1:2.2, red). Expansions of two regions are shown, with most peaks in fast or intermediate exchange; B, Chemical shift perturbations (CSP) are shown for backbone NH groups. The red line indicates the mean CSP, plus one standard deviation. Residues that disappeared in the presence of Cdc42 were assigned a CSP of 0.1 and are indicated with open bars. Those that were not traceable due to overlap are marked with an asterisk. Residues with disappeared peaks in ^{13}C HSQC experiments are marked on the chart with green asterisks. Secondary structure elements are indicated below the graph; C, The residues with significantly affected backbone and sidechain groups are highlighted on an NMR structure of free Cdc42Δ7Q61L·GMPPNP: those that are buried are coloured dark blue, while those that are

solvent accessible are coloured red. Residues with either sidechain or backbone groups affected are coloured blue if buried and yellow if solvent accessible. Residues without information from shift mapping are coloured grey. The flexible switch regions are circled.

FIGURE 6. Model of Cdc42-HR1 complex. A, A representative model of the Cdc42-HR1 complex from the cluster closest to the lowest energy model produced using HADDOCK (67). Residues of Cdc42 that are affected in the presence of the HR1 domain but are not in close proximity to it are coloured in red and labelled, B, The structure of Rac1 in complex with the HR1b domain of PRK1 (46) (PDB Code: 2RMK), C, A sequence alignment of RhoA, Cdc42 and Rac1. Contact residues of RhoA and Rac1 to PRK1 HR1a and HR1b respectively are coloured cyan. Residues of Cdc42 that disappear or show chemical shift changes in the presence of TOCA1 are coloured cyan if also identified as contacts in RhoA and Rac1 and yellow if they are not. Residues equivalent to Rac1 and RhoA contact sites but are invisible in free Cdc42 are grey; D, Regions of interest of the Cdc42-HR1 domain model. The four lowest energy structures in the chosen HADDOCK cluster are shown overlaid, with the residues of interest shown as sticks and labelled. Cdc42 is shown in cyan and TOCA1 in purple.

FIGURE 7. The N-WASP GBD displaces the TOCA1 HR1 domain. A, The model of the Cdc42-TOCA1 HR1 domain complex overlaid with the Cdc42-WASP structure. Cdc42 is shown in green and TOCA1 in purple. The core CRIB region of WASP is shown in red, whilst its basic region is in orange and the C-terminal region required for maximal affinity in cyan. A semi-transparent surface representation of Cdc42 and WASP is shown overlaid with the cartoon; B, Competition SPA experiments carried out with indicated concentrations of the N-WASP GBD construct titrated into 30 nM GST-ACK or GST-WASP GBD and 30 nM Cdc42Δ7Q61L·[^{3}H]GTP; C, Selected regions of the ^{15}N-HSQC of 145 μM Cdc42Δ7Q61L·GMPPNP with indicated ratios of the TOCA1 HR1 domain, the N-WASP GBD or both, showing that the TOCA HR1 domain does not displace the N-WASP GBD; D, Selected regions of the ^{15}N-HSQC of 600 μM of the TOCA1 HR1 domain in complex with Cdc42 in the absence and presence of the N-WASP GBD, showing displacement of Cdc42 from the HR1 domain by N-WASP.

FIGURE 8. Actin polymerisation downstream of Cdc42-N-WASP-TOCA1 is inhibited by excess N-WASP GBD but not by the TOCA1 HR1 domain. Fluorescence curves showing actin polymerisation in the presence of increasing concentrations of N-WASP GDB or TOCA1 HR1 domain as indicated. Maximal rates of actin polymerisation derived from the linear region of the curves are represented in bar charts below. Error bars show standard error of the mean.

FIGURE 9. A simplified model of the early stages of Cdc42/N-WASP/TOCA1-dependent actin polymerisation. Step1: TOCA1 is recruited to the membrane via its F-BAR domain and/or Cdc42 interactions. F-BAR oligomerization is expected to occur following membrane binding but a single monomer is shown for clarity. Step 2: N-WASP exists in an inactive, folded conformation. The TOCA1 SH3 domain interacts with N-WASP, causing an activator allosteric effect. The HR1^{TOCA1}-Cdc42 and SH3^{TOCA1}-N-WASP interactions position Cdc42 and N-WASP for binding. Step3: Electrostatic interactions between Cdc42 and the basic region upstream of the CRIB initiate Cdc42-N-WASP binding. Step4: The core CRIB binds with high affinity while the region C-terminal to the CRIB displaces the TOCA1 HR1 domain and increases the affinity of the N-WASP-Cdc42 interaction further. The VCA domain is released for downstream interactions and actin polymerisation proceeds. WH1 = WASP homology 1 domain, CRIB = Cdc42- and Rac1-Interactive binding region, PP = Proline-rich region, VCA = Verprolin homology, cofilin homology, acidic region.

TABLE 1. Experimental Restraints and Structural Statistics.

Experimental restraints			
Distance restraints:			
Total non-degenerate	2602		
Unambiguous	1845		
Ambiguous	757		
Dihedral angle restraints	164		
		<SA> [a]	**<SA>** [b]
Coordinate precision for well-ordered regions			
RMSD of backbone atoms (342-379, 386-419) (Å)		0.67 ± 0.14	0.46
RMSD of all heavy atoms (342-379, 386-419) (Å)		1.10 ± 0.12	0.96
Ramachandran analysis for all residues			
Residues in most favoured regions:		99.4 %	96.1 %
Residues in additionally allowed regions:		0.6 %	3.9 %
Residues in disallowed regions:		0 %	0 %
RMS deviations for all residues			
from the experimental restraints:			
NOE distances (Å)		0.011 ± 0.0027	0.011
Dihedral angles (°)		0.14 ± 0.067	0.18
from idealised geometry:			
Bonds (Å)		0.0027 ± 0.00009	0.00269
Angles (°)		0.434 ± 0.012	0.427
Impropers (°)		1.025 ± 0.073	1.11

[a] <SA> represents the average RMS deviations for the ensemble of 35 structures.
[b] <SA> represents values for the structure that is closest to the mean.

Figure 1

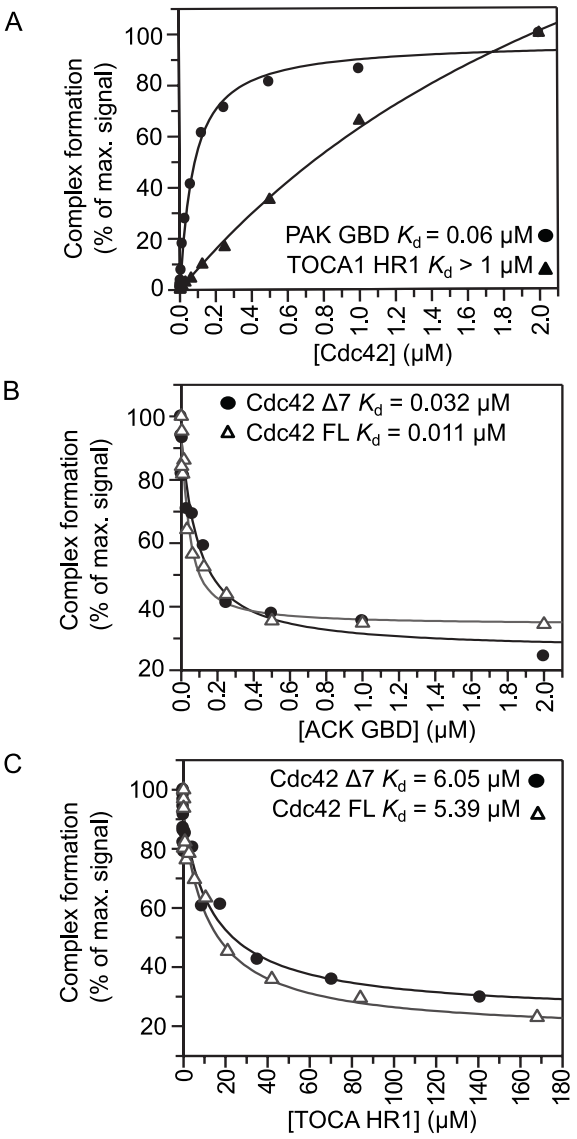
A
Complex formation (% of max. signal)
PAK GBD K_d = 0.06 µM
TOCA1 HR1 K_d > 1 µM
[Cdc42] (µM)
B
Cdc42 Δ7 K_d = 0.032 µM
Cdc42 FL K_d = 0.011 µM
Complex formation (% of max. signal)
[ACK GBD] (µM)
C
Cdc42 Δ7 K_d = 6.05 µM
Cdc42 FL K_d = 5.39 µM
Complex formation (% of max. signal)
[TOCA HR1] (µM)

Figure 2

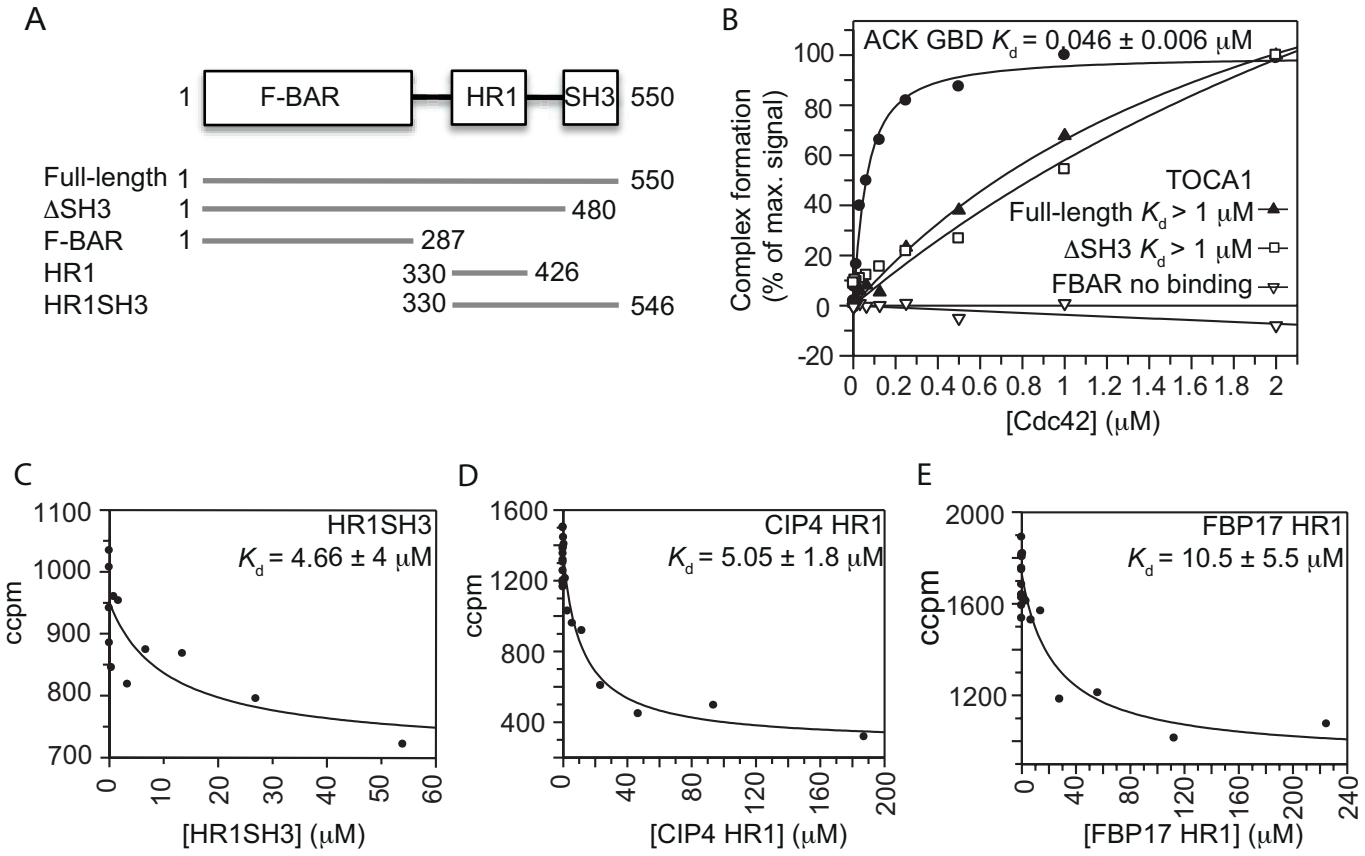
A
1
F-BAR
HR1
SH3
550
Full-length 1 550
ΔSH3 1 480
F-BAR 1 287
HR1 330 426
HR1SH3 330 546
B
ACK GBD K_d = 0.046 ± 0.006 μM
Complex formation (% of max. signal)
TOCA1
Full-length K_d > 1 μM
ΔSH3 K_d > 1 μM
FBAR no binding
[Cdc42] (μM)
C
HR1SH3
K_d = 4.66 ± 4 μM
ccpm
[HR1SH3] (μM)
D
CIP4 HR1
K_d = 5.05 ± 1.8 μM
ccpm
[CIP4 HR1] (μM)
E
FBP17 HR1
K_d = 10.5 ± 5.5 μM
ccpm
[FBP17 HR1] (μM)

Figure 3

A

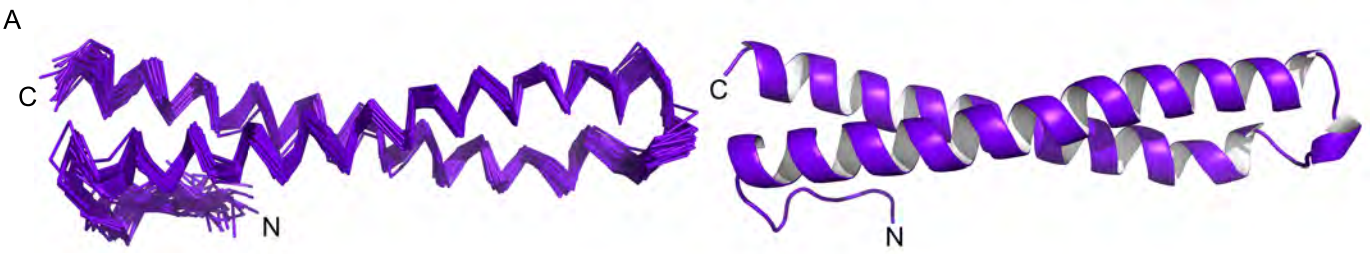

B

```
TOCA1  330 ------KGPALEDFSHLPPEQRRKRLQQRIDELSRELQKEMDQKDALNKMKDVYEK 379
CIP4   332 ----------TEDFSHLPPEQQRKRLQQQLEERSRELQKEVDQREALKKMKDVYEK 377
HR1a     6 VQSEPRSWSLLEQLGLAGADLAAPGVQQQLELERERLRREIRKELKLKEGAENLRR 61
HR1b   122 ------------------------ATNLSRVAGLEKQLAIELKVKQGAENMIQ 150

TOCA1  380 NP-QMG----DPS-SLHPKIAETTSNIERLRMEIHKNEAWLSEVEGKV-SQRSE   426
CIP4   378 TP-QMG----DPA-SLEPQIAETLSNIERLKLEVQKYEAWLAEAESRVLSNRGD   425
HR1a    62 ATTDLG----RSLGPVELLLRGSSRRLDLLHQQLQELHAHVVLPDPAAT-----   106
HR1b   151 TYSNGSTKDRKLLLTAQQMLQDSKTKIDIIRMQLRRALQADQLENQAAP-----   199
```

C

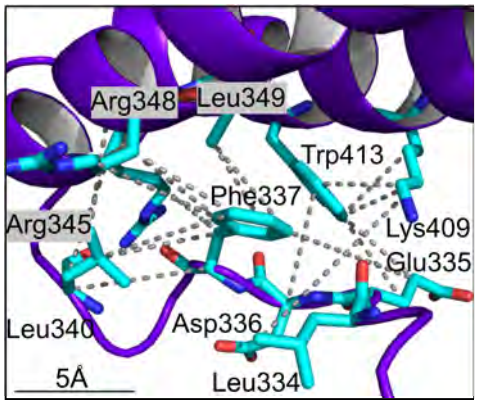

D

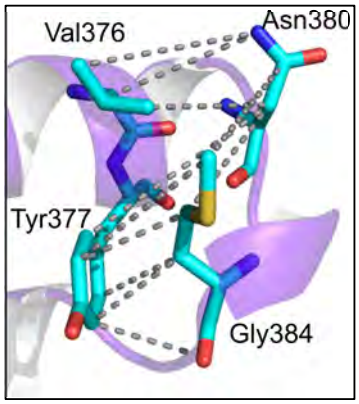

Figure 4

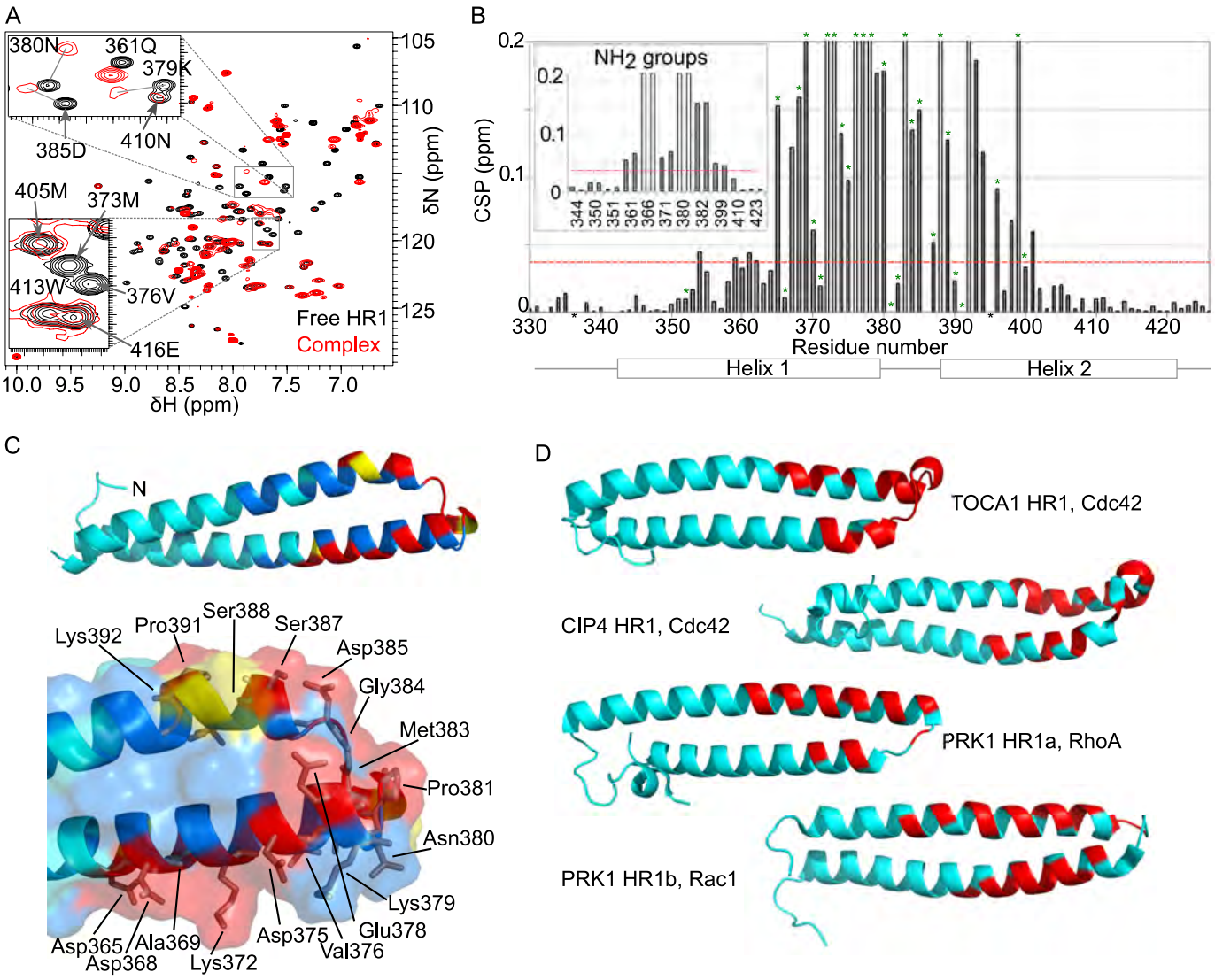
A
380N
361Q
379K
385D
410N
405M
373M
413W
376V
416E
Free HR1
Complex
δH (ppm)
δN (ppm)
B
NH2 groups
CSP (ppm)
Residue number
Helix 1
Helix 2
C
N
Lys392
Pro391
Ser388
Ser387
Asp385
Gly384
Met383
Pro381
Asn380
Lys379
Glu378
Val376
Asp375
Ala369
Asp365
Asp368
Lys372
D
TOCA1 HR1, Cdc42
CIP4 HR1, Cdc42
PRK1 HR1a, RhoA
PRK1 HR1b, Rac1

Figure 5

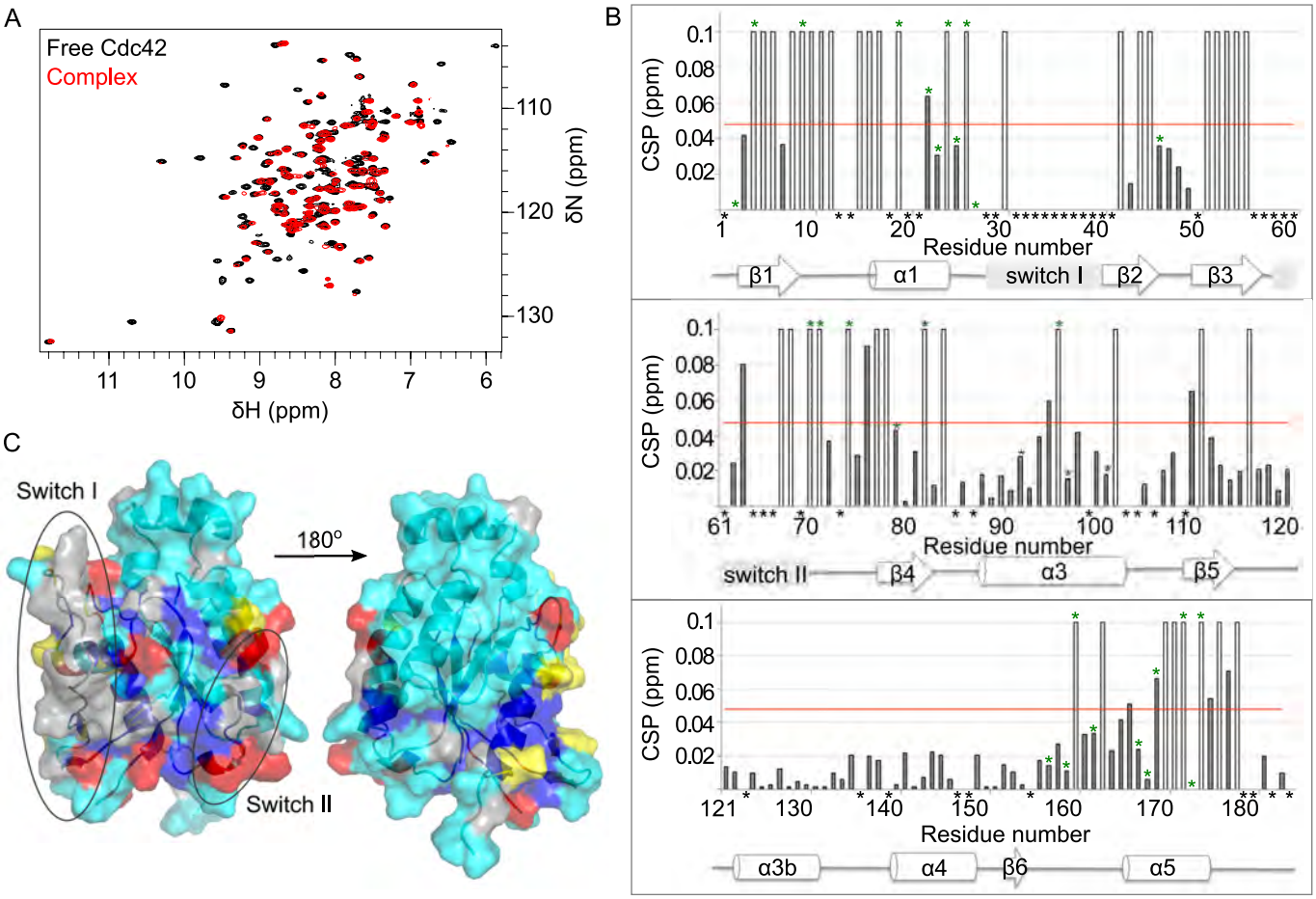
A
Free Cdc42
Complex
δH (ppm)
δN (ppm)
B
CSP (ppm)
Residue number
β1
α1
switch I
β2
β3
switch II
β4
α3
β5
α3b
α4
β6
α5
C
Switch I
180°
Switch II

Figure 6

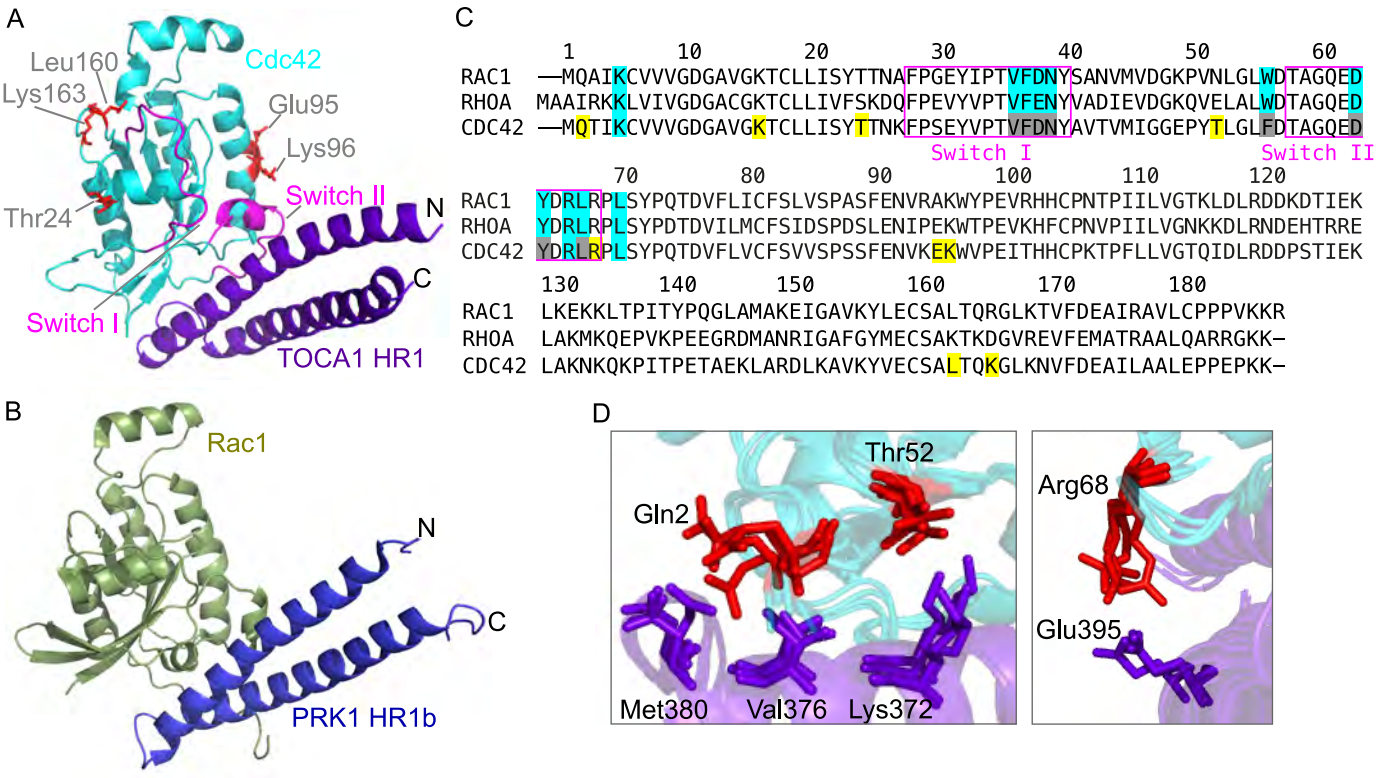
A
Leu160
Cdc42
Lys163
Glu95
Lys96
Switch II
Thr24
N
C
Switch I
TOCA1 HR1
B
Rac1
N
C
PRK1 HR1b
C
1 10 20 30 40 50 60
RAC1 —MQAIKCVVVGDGAVGKTCLLISYTTNAFPGEYIPTVFDNYSANVMVDGKPVNLGLWDTAGQED
RHOA MAAIRKKLVIVGDGACGKTCLLIVFSKDQFPEVYVPTVFENYVADIEVDGKQVELALWDTAGQED
CDC42 —MQTIKCVVVGDGAVGKTCLLISYTTNKFPSEYVPTVFDNYAVTVMIGGEPYTLGLFDTAGQED
Switch I
Switch II
70 80 90 100 110 120
RAC1 YDRLRPLSYPQTDVFLICFSLVSPASFENVRAKWYPEVRHHCPNTPIILVGTKLDLRDDKDTIEK
RHOA YDRLRPLSYPDTDVILMCFSIDSPDSLENIPEKWTPEVKHFCPNVPIILVGNKKDLRNDEHTRRE
CDC42 YDRLRPLSYPQTDVFLVCFSVVSPSSFENVKEKWVPEITHHCPKTPFLLVGTQIDLRDDPSTIEK
130 140 150 160 170 180
RAC1 LKEKKLTPITYPQGLAMAKEIGAVKYLECSALTQRGLKTVFDEAIRAVLCPPPVKKR
RHOA LAKMKQEPVKPEEGRDMANRIGAFGYMECSAKTKDGVREVFEMATRAALQARRGKK–
CDC42 LAKNKQKPITPETAEKLARDLKAVKYVECSALTQKGLKNVFDEAILAALEPPEPKK–
D
Thr52
Gln2
Met380
Val376
Lys372
Arg68
Glu395

Figure 7

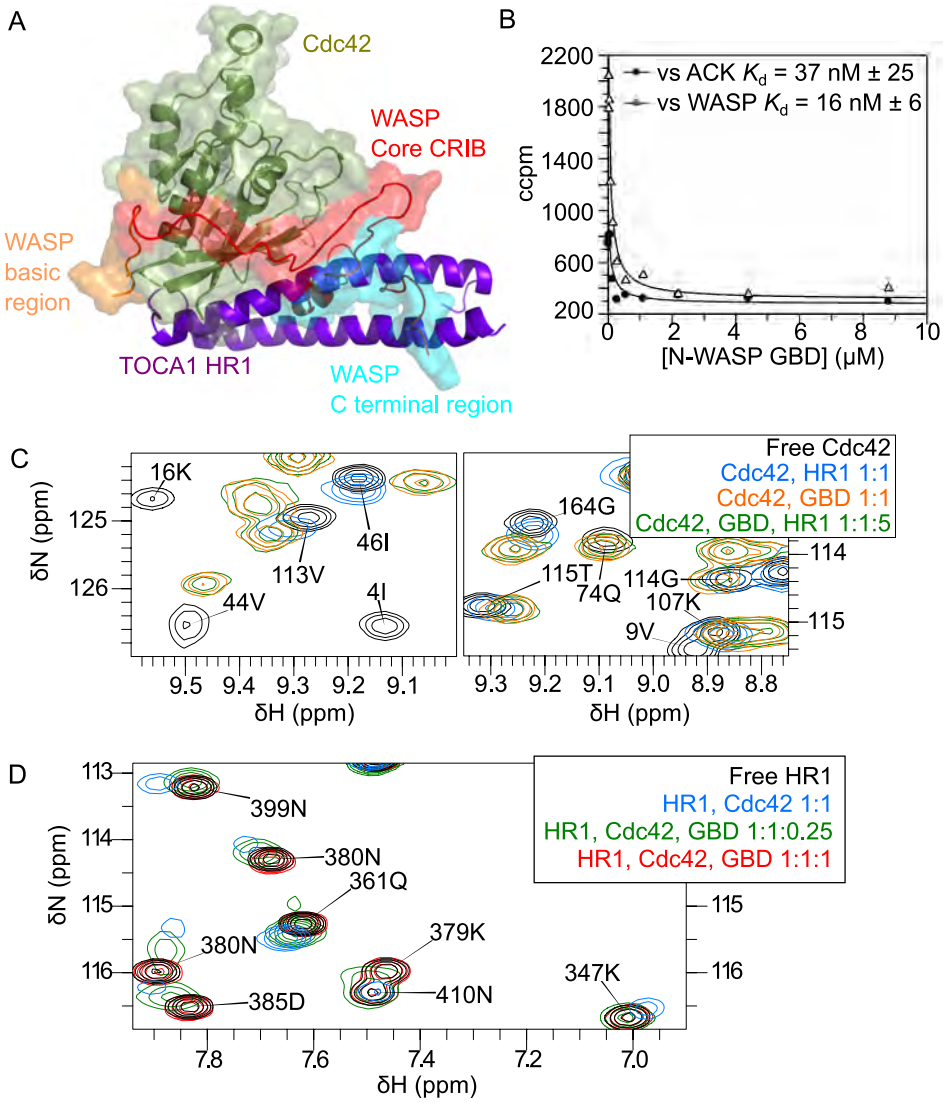
A
Cdc42
WASP
Core CRIB
WASP
basic
region
TOCA1 HR1
WASP
C terminal region
B
vs ACK K_d = 37 nM ± 25
vs WASP K_d = 16 nM ± 6
ccpm
[N-WASP GBD] (μM)
C
16K
46I
113V
44V
4I
164G
115T
74Q
114G
107K
9V
Free Cdc42
Cdc42, HR1 1:1
Cdc42, GBD 1:1
Cdc42, GBD, HR1 1:1:5
δN (ppm)
δH (ppm)
D
399N
380N
361Q
380N
379K
385D
410N
347K
Free HR1
HR1, Cdc42 1:1
HR1, Cdc42, GBD 1:1:0.25
HR1, Cdc42, GBD 1:1:1
δN (ppm)
δH (ppm)

Figure 8

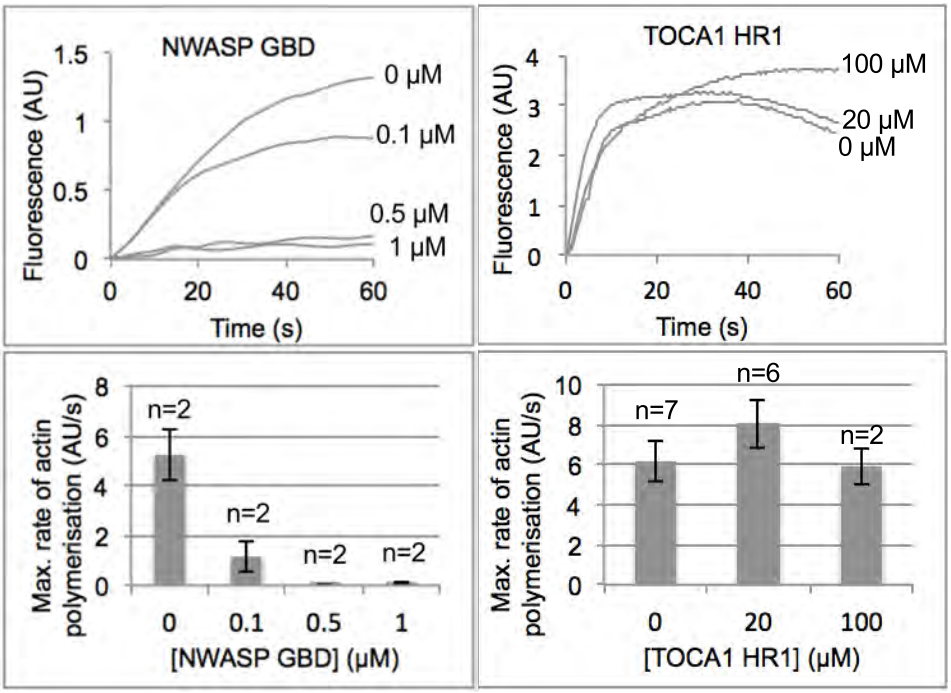
NWASP GBD
Fluorescence (AU)
1.5
1
0.5
0
0 μM
0.1 μM
0.5 μM
1 μM
0
20
40
60
Time (s)
TOCA1 HR1
Fluorescence (AU)
4
3
2
1
0
100 μM
20 μM
0 μM
0
20
40
60
Time (s)
Max. rate of actin polymerisation (AU/s)
8
6
4
2
0
n=2
n=2
n=2
n=2
0
0.1
0.5
1
[NWASP GBD] (μM)
Max. rate of actin polymerisation (AU/s)
10
8
6
4
2
0
n=7
n=6
n=2
0
20
100
[TOCA1 HR1] (μM)

Figure 9

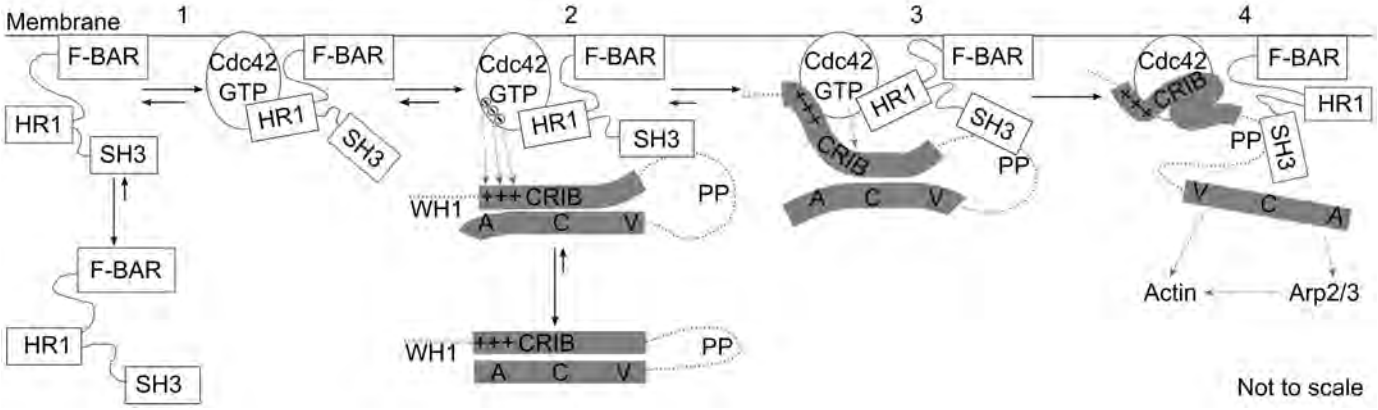
Membrane
1
2
3
4
F-BAR
HR1
SH3
Cdc42
GTP
WH1
+++ CRIB
A C V
PP
Actin
Arp2/3
Not to scale